

Glacier Image Velocimetry: an open-source toolbox for easy and rapid calculation of high-resolution glacier-velocity fields

Maximillian Van Wyk de Vries^{1,2} and Andrew D. Wickert^{1,2}

¹Department of Earth & Environmental Sciences, University of Minnesota, Minneapolis, MN

²Saint Anthony Falls Laboratory, University of Minnesota, Minneapolis, MN

Correspondence: Maximillian Van Wyk de Vries (vanwy048@umn.edu)

Abstract. We present ‘Glacier Image Velocimetry’ (GIV), an open-source and easy-to-use software toolkit for rapidly calculating high spatial resolution glacier-velocity fields. Glacier ice velocity fields reveal flow dynamics, ice-flux changes, and (with additional data and modelling) ice thickness. Obtaining glacier-velocity measurements over wide areas with field techniques is labour intensive and often ~~a safety risk~~associated with safety risks. Recent increased availability of high-resolution, short-repeat-time optical imagery allow us to obtain ice displacement fields using ‘feature tracking’ based on ~~the presence of matching~~ persistent irregularities on the ice surface between images, and hence, surface velocity over time. GIV is fully parallelized, and automatically detects, filters, and extracts velocities from large datasets of images. Through this coupled toolchain and an easy-to-use GUI, GIV can rapidly analyze hundreds to thousands of image pairs on a laptop or desktop computer. We present four example applications of the GIV toolkit in which we complement a glaciology field campaign (Glaciar Perito Moreno, Argentina) and calculate the velocity fields of small mid-latitude (Glacier d’Argentière, France) and ~~very large (Vavilov ice cap, Russia)~~tropical glaciers (Volcán Chimborazo, Ecuador), as well as ~~a tropical ice cap (Volcán Chimborazo, Ecuador)~~very large glaciers (Vavilov Ice Cap, Russia). Fully commented MATLAB code and a standalone app for GIV are available from GitHub and Zenodo at github.com/MaxVWDV/glacier-image-velocimetry.

Copyright statement. Includes imagery © Google Earth

1 Introduction

Satellite imagery revolutionized our ability to study changes ~~on the surface of our planet. Satellite datasets now routinely support storm and drought evaluations (Klemas, 2009; Rhee et al., 2010; AghaKouchak et al., 2015), volcanic activity monitoring (Wright et al., 2002; Harris, 2013), and landslide hazard analysis (Metternicht et al., 2005; Tralli et al., 2005; Mare and Hovius, 2015).~~ In glaciology, remote sensing has enabled global glacier inventories (Pfeffer et al., 2014; Earl and Gardner, 2016) as well as ~~high-resolution elevation models and image mosaics of the Antarctic and Greenland ice sheets (Bindshadler et al., 2008; Hui et al., 2013; F~~ With temperatures consistently rising throughout much of the globe, these images also provide an important temporal record

of changes in ice extent and volume, as well as an in glacier extent, volume, and surface velocities, and is an effective tool for communicating these changes to the broader public (Scambos et al., 2007; Stocker et al., 2013; Howat et al., 2019).

The use of imagery is not limited to mapping changes in glacial extent. The snowline on temperate glaciers, easily visible from end-of-melt-season images, defines the equilibrium-line altitude, thereby delineating glacier accumulation and ablation areas (Bamber and Rivera, 2007; Rabatel et al., 2008; Yuwei et al., 2014). Identifying both seasonal and annual changes in snowline can provide important information about local winter precipitation, summer air temperatures, and longer-term glacier mass changes (Bakke and Nesje, 2011).

Velocity measurements permit (Scambos et al., 1992; Rignot et al., 2011; Heid and Kääb, 2012a; Stocker et al., 2013; Howat et al., 2019).

Glacier-velocity measurements enable scientists to map glacier divides and drainage basins (Davies and Glasser, 2012; Pfeffer et al., 2014; Mouginot and Rignot, 2015) and, track changes in surface melt production and accumulation (Mote, 2007; Sneed and Hamilton, 2007). Advancing techniques to remotely sense glaciers — and particularly their velocities — continues to provide new avenues to, and address key questions in about ice dynamics and the future of glaciers under a changing climate (Stearns et al., 2008; Wal et al., 2008; Rignot et al., 2011; Willis et al., 2018) (Stearns et al., 2008; ?; Rignot et al., 2011; Willis et al., 2018).

Even the earliest glaciologists identified that glaciers may flow as viscous fluids (Forbes, 1840, 1846; Bottomley, 1879; Nye, 1952), and later that glacier-surface motions reflect a complex interplay between internal deformation, basal sliding, and deformation of subglacial sediments (Deeley and Parr, 1914; Weertman, 1957; Kamb and LaChapelle, 1964; Nye, 1970; Fowler, 2010). Sudden peaks in velocity may result from a sudden change in basal sliding, perhaps as the result of changing englacial hydrology. Long-term speedups or slowdowns may reflect climatic shifts or drainage reorganizations. Such changes reflect a combination of glacier mass balance and basal conditions – including time-varying hydrology – both of which may respond to climate. Widespread measurement of glacier-surface velocities, a key constraint on glacier dynamics, has however only become possible with the advent of satellite-based remote sensing (e.g. Bindschadler and Scambos, 1991; Scambos et al., 1992).

Deriving glacier velocities from satellite imagery is possible through an image-analysis technique known as ‘feature tracking’, ‘image cross correlation’, or ‘particle image velocimetry’. The latter term, ‘particle image velocimetry’, describes a well-established technique in fluid dynamics, typically involving the use of a high-speed digital camera to track the motion of tracers within a fluid in a laboratory setting (Buchhave, 1992; Grant, 1997; Raffel et al., 2018). These ideas were first carried over to the field of glaciology by Bindschadler and Scambos (1991) and Scambos et al. (1992) to evaluate the flow velocity of a portion of an Antarctic ice stream. Since that time, the increasing abundance and availability of imagery has facilitated expanded use of feature-tracking-based velocimetry techniques. With the release of the full Landsat data archive and launch of Sentinel-2, 10–30-m pixel resolution imagery of any given location is now available at sub-weekly repeat coverage intervals. A number of studies apply this exceptional archive to map velocity fields across the major ice sheets as well those of many glaciers around the world (Gardner et al., 2018; Millan, 2019).

Prior to the advent of remote sensing, spatially distributed measurements of glacier flow velocities required lengthy field campaigns (Meier and Tangborn, 1965; Hooke et al., 1989; Chadwell, 1999; Mair et al., 2003). Nowadays full 2D flow-velocity maps may be readily calculated from a variety of optical and radar-based satellite imagery (Heid and Kääb, 2012b; Fahnestock et al., 2016). For this toolbox we focus on optical imagery products due to their ease of access, limited need for

pre-processing and high spatial and temporal resolution (Drusch et al., 2012; Heid and Kääb, 2012b, a; Kääb et al., 2016; Darji et al., 2018).

A number of tools exist to derive displacements from imagery, as partially reviewed by Heid and Kääb (2012a); Jawak et al.

(2018) and Darji et al. (2018). [These include CARST \(Cryosphere and Remote Sensing Toolkit: Willis et al., 2018\), COSI-corr \(Co-registration of Optically Sensed Images and Correlation: Leprince et al., 2007b\), AutoRIFT \(Autonomous Repeat Image Feature Tracking: Leprince et al., 2007b\), ImGRAFT \(Image Georectification and Feature Tracking: Messerli and Grinsted, 2015\), and SenDiT \(the Sentinel-2 Displacement Tool: Leprince et al., 2007b\). CARST contains a mixture of Python and Bash scripts used to monitor changes in glaciers, and includes feature-tracking and ice-elevation-change-monitoring tools \(Willis et al., 2018; Zheng et al., 2018, 2019a\). COSI-Corr is a flexible co-registration and feature-tracking tool written in IDL, implemented in the ENVI GIS package, and initially used for measuring co-seismic deformation. Auto-RIFT is a Python-based feature-tracking algorithm \(Gardner et al., 2018\). ImGRAFT is a MATLAB-based toolbox for georectifying and feature-tracking of ground based imagery, and may also be used on satellite imagery. SenDiT provides a platform to automatically download and generate velocity maps based on Sentinel-2 data, using a Python interface with bindings to the C- and Fortran-based *imcorr* toolbox \(Scambos et al., 1992\) for feature-tracking calculations. In addition, near-global ice-velocity maps are calculated in near-real time from Landsat and other freely available satellite data sources \(Scambos, 2016; Gardner et al., 2020\): GoLIVE using PyCorr \(Scambos, 2016\), and ITS LIVE using Auto-RIFT \(Gardner et al., 2020\).](#)

Table 1 presents a non-exhaustive list of ~~software packages available online. Our objective with the~~ feature-tracking software packages. In some circumstances, GIV will not be the most suitable feature-tracking tool depending on user's requirements. For example, users who need to manually perform prior image co-registration (e.g. with airphotos) may wish to the built-in workflow in COSI-Corr. The objective of 'Glacier Image Velocimetry' (GIV) toolbox presented here is ~~to not to compete with or replace these other tools. Rather, GIV aims to to~~ provide an easy-to-use, flexible, and ~~efficient tool that can robustly~~ alternative. GIV may be used to derive high spatial ~~resolution and monthly and~~ temporal resolution surface-velocity maps of ~~any glacier~~ glaciers of all scales. The following section will run through the basics of the image-feature-tracking techniques and advances built into GIV.

2 Methods and model setup

The fundamental idea ~~behind of~~ feature tracking is based on techniques used to co-register images: the properties of two images are compared in order to identify the best-fit location of one image within the other (Scambos et al., 1992; Thielicke and Stamhuis, 2014; Messerli and Grinsted, 2015). In feature tracking, including in GIV, individual images are divided into a grid of smaller images (referred to as 'chips'). We compare each individual 'chip' from the first image (I1) to a surrounding portion within a second image (I2), and find the best matching portion of I2. If no displacement has occurred between the two images, the best-fitting portion of I2 will have the same location as the original 'chip' on I1 (excluding any georeferencing or distortion-related errors). However, if any motion has occurred between the two images, the corresponding best matching 'chip' within I2 will be displaced relative the original location within I1. We may then determine the bulk displacement in pixels

90 between the original I1 ‘chip’ and best match I2 ‘chip’. The correlation coefficients between the original chip and surrounding area within I2 are also calculated. This allows a Gaussian curve to be fit to this grid in order to determine the peak location at sub-pixel accuracy. Repeating this routine for every chip within the original image allows a 2D surface velocity field to be derived.

When initially developed for use in laboratory-based fluid dynamics, the camera, lighting, and tracer-particle conditions
 95 were all closely constrained (Grant, 1997; Raffel et al., 2018). On glaciers, features change over time as crevasses open and close, snow drifts, and ablation exposes new surfaces. In addition, the satellite may acquire imagery from slightly different locations and angles with each pass, and lighting conditions depend strongly on the time of day and year, as well as [degree of shadowing and](#) local weather conditions (Berthier et al., 2005; Kääb et al., 2016). This complexity raises additional problems in the use of this technique for deriving glacier velocities, and makes it entirely unusable in some cases (e.g. images too far
 100 spaced in time relative to the speed of the glacier ~~surface~~ for image pairs to retain any coherence). These problems can be mitigated though a combination of image pre-filtering, comparison between adjacent velocity maps, and outlier filtering. We also refer readers to chapters 2 and 4 of Altena (2018) for detailed discussion on these topics. The Glacier Image Velocimetry toolbox makes use of these methods, with a particular emphasis on noise reduction in individual velocity map outputs through the use of large datasets. Figure 1 presents the overall model setup and order of operations.

105 2.1 Model pre-processing

Prior to running the feature-tracking algorithms, the satellite images are first loaded into the workspace and filtered. The user interface will prompt the user to enter the coordinates of the images (minimum and maximum latitude and longitude), and to select a given folder in which the images are stored. These images can be .png, .jpg, or .geotiff files of the area, with each file name being the date of image acquisition (in yyyyymmdd format). In the case of a geotiff input, GIV will automatically
 110 load the geographic information from the input. GIV will then extract the dates from the file names, calculate time between images, and load the raw image data into an array for further processing. The user also inputs a modified image with glaciers of interest converted to pure white (RGB 255,255,255). This image is loaded by GIV and converted into a binary mask with areas within (1) and outside (0) the computational region. The size and resolution of images are also automatically calculated and re-sampled to a common resolution, such that images from different satellites may be combined into the same dataset.

115 Following this, GIV filters the images according to user-defined settings. GIV includes a range of filters in order to reduce the effect of unwanted noise (e.g. clouds and shadows) and emphasize trackable features (e.g. crevasses, snowdrifts, supraglacial debris). In particular we include high-pass, Sobel, and Laplacian filter options to emphasize short-wavelength features and edges, as well as intensity-capping and contrast-limited histogram-equalization filters to improve image contrast (Sveen, 2004; Thielicke and Stamhuis, 2014; Gardner et al., 2018). We also include a variation of the orientation filter (Fitch et al., 2002)
 120 named ‘near anisotropic orientation filter’ (NAOF). We define this filter as:

$$I_f = \sum_{i=1}^4 \cos[\arctan 2(I_o * \alpha_i, I_o * R[\alpha_i])] \quad (1)$$

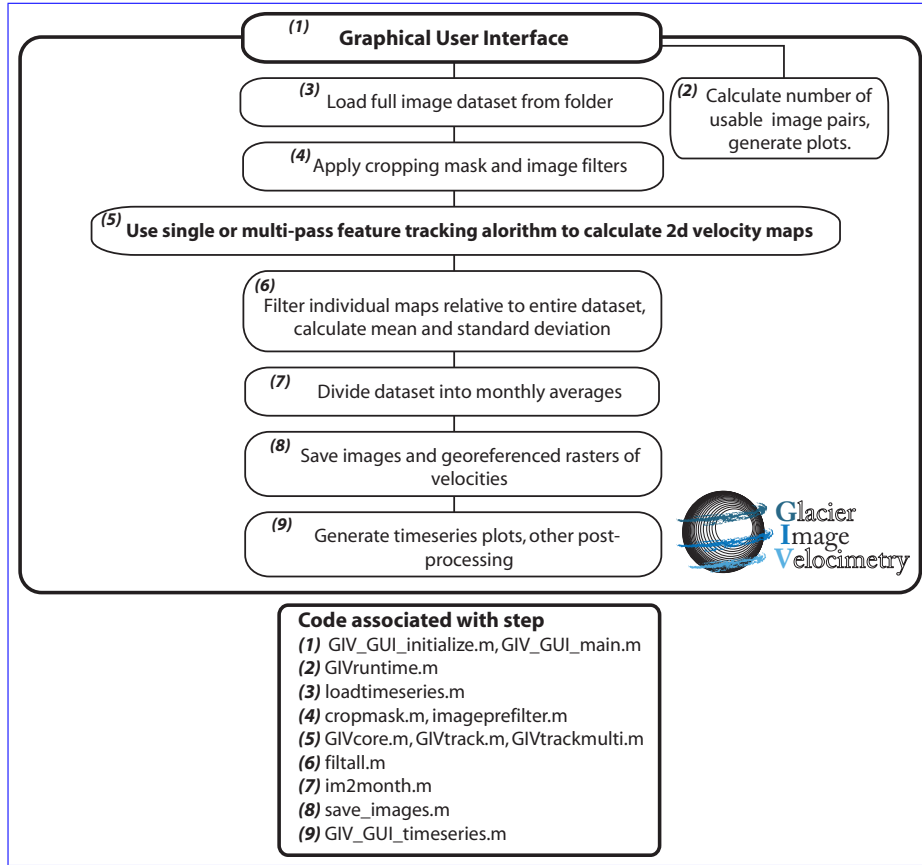


Figure 1. Flowchart describing the Glacier Image Velocimetry toolbox design. Names of the code files associated with each step are given for reference (and are available in the linked Zenodo repository). The feature-tracking step is shown in bold. Note that users-can-access the source code is open source, but that accessing it is not necessary for running GIV. Users may enter all parameters-parameter options into fields in the user interface, with subsequent steps automatically performed by the toolbox.

With I_f the filtered image, I_o the original image, α representing four different convolution matrices oriented at 45 degrees from each other using the 8 adjacent pixels, $\arctan 2(x, y)$ representing the four-quadrant arctangent (also called the two-argument arctangent), $x * y$ representing a two dimensional matrix convolution, and $R[x]$ representing a 90 degree matrix rotation. This filter works by summing differently angled orientation filters together in order to recover a ‘pseudo-feature’ with the same location as the original feature, but with an increased contrast between the feature and the background, and homogenized magnitude (Fitch et al., 2002; Kobayashi and Otsu, 2008). Information on absolute pixel color magnitude is discarded, with only information on color gradients preserved. A similar result may be obtained by convolving the original image with a single convolution matrix summing the four directional filters, but this normalizes all features to a single magnitude and results in a larger number of false matches. The NAOF has the advantages of (a) strongly increasing the contrast between features and background; (b) removing contrast differences between clouded, shadowed, and clear areas; and (c) preserving feature

location and uniqueness. Figure 2 shows examples of how this filter is able to recover features from challenging images. Many glaciated areas remain cloud covered and shadowed for much of the year, so being able to recover partial velocity fields from these images can greatly increase the size of potential datasets. Note that no amount of filtering can improve certain images, such as those in which cloud cover is too thick for the glacier surface to be visible. An evaluation of the quality of velocity maps derived from different image filters is provided in the supplementary material (figures S1-S16). These show that NAOF, contrast-limited histogram-equalization and high-pass filtering provide a major improvement over raw imagery.

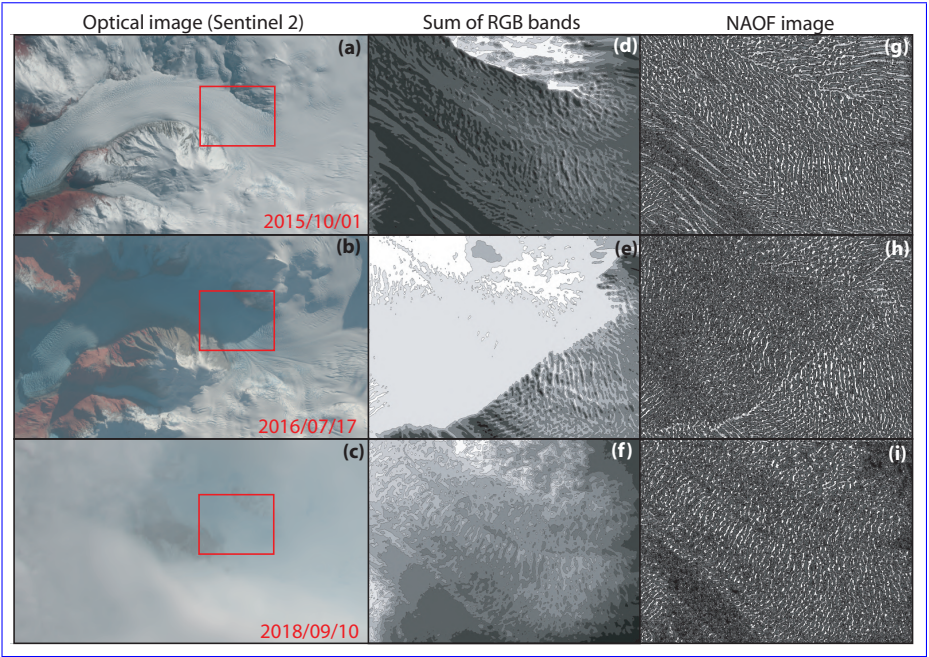


Figure 2. Comparison between raw optical images, band-summed images and NAOF-filtered images for a clear image (a, d, g), a heavily shadowed image (b, e, h), and a cloudy image (c, f, i) of Amalia glacier, Patagonia (-50.92 S, -73.56 W). Note how despite the complexity, the NAOF images recover a clear and easily traceable feature pattern on the surface of the glacier that is suitable for obtaining velocities. The shadow line leaves an artefact in h, but is a marked improvement on the lack of features in the shaded area in e. Images from Sentinel-2.

2.2 Velocity calculations

2.2.1 Frequency-domain matching

The central part of any ~~feature-tracking~~ feature-tracking code involves matching a small region of one image ('chip') with a surrounding region of a second image ('search area'). The 'chip' is matched to the 'search area' through two-dimensional cross correlation, which may be performed in the spatial or frequency domain (Thielicke and Stamhuis, 2014; Altena, 2018). Matching in the spatial domain ('normalized cross correlation') may better account for feature distortion or shear, and may have a higher accuracy (Thielicke and Stamhuis, 2014). Frequency domain methods ('frequency cross correlation') generally

145 benefit from a greater computational efficiency, as the correlation matrix is calculated across the whole domain in one operation. We implement frequency-domain matching in GIV, as feature distortion is minimal in most glaciers and it has been found to perform well in prior studies (e.g., Heid and Kääb, 2012a). We refer readers to Thielicke and Stamhuis (2014) and chapter 4 of Altena (2018) for more details on these topics.

Frequency cross correlation involves calculating the correlation between the ‘chip’ and ‘search area’ in the frequency do-
150 main. This is done by converting both the ‘chip’ and ‘search area’ to the frequency domain using a fast Fourier transform (FFT), calculating the pointwise product between these two matrices and converting the resulting similarity matrix back to the spatial domain with an inverse FFT (IFFT). This step is repeated on each chip within the original image, and is the most computationally expensive of the entire process.

~~Displacements may be derived from an image pair either with a single pass across the images, or with multiple passes
155 with gradually reducing window sizes (Thielicke and Stamhuis, 2014; Raffel et al., 2018). Single-pass methods generally have the advantage of generally being faster at coarse resolutions and are less at risk of smearing one erroneous value over a larger area. Multi-pass methods update displacement estimates over multiple iterations, refining initial coarse-window-size displacement calculations using progressively smaller window sizes. Multi-pass methods combine the advantages of better feature matching at large window sizes with the higher spatial resolution of small window sizes. Both methods are integrated
160 into GIV, with a single-pass method based on ImGRAFT (Messerli and Grinsted, 2015) and a 3-iteration multi-pass algorithm modified from matpiv (Sveen, 2004). Both functions have been tested in a number of previous studies, with matpiv being used extensively in fluid-dynamics research (e.g., Sveen and Cowen, 2004; Sveen, 2004; Lee et al., 2017; Oertel and Süfke, 2020). An experiment evaluating the difference between a normalized cross-correlation algorithm and the multipass frequency domain cross-correlation in GIV is given in the supplementary material. We find that the multipass frequency domain algorithm
165 produces velocity maps with higher signal to noise ratio than the normalized cross-correlation algorithm across test scenarios with a range of cloud cover.~~

~~Comparison between raw optical images, band-summed images and NAOF-filtered images for a clear image (a, d, g), a heavily shadowed image (b, e, h), and a cloudy image (c, f, i). Note how despite the complexity, the NAOF images recover a clear and easily traceable feature pattern on the surface of the glacier that is suitable for obtaining velocities. The shadow line
170 leaves an artefact in h, but is a marked improvement on the lack of features in the shaded area in e. Images from Sentinel-2.~~

~~GIV is~~ GIV is written in MATLAB. Despite being a high-level interpreted programming language, MATLAB performs FFT calculations using precompiled C and Fortran bindings for the FFTW library (Frigo and Johnson, 1998, 2005). Due to this being the rate-limiting step in ~~feature tracking~~ feature-tracking calculations (>90% of computation time in most cases), such code may be written in MATLAB with few performance issues relative to other programming languages.

175 2.2.2 Parallel computing

As the feature-tracking correlation between two images inherently requires a large number of FFT and IFFT operations, this step has limited potential for further optimization. Computation time may instead be decreased by deriving displacement fields from different image pairs in parallel rather than in series. This requires a slightly different code design: First, GIV detects the

number of physical cores on the user's computer and starts a parallel pool(~~users may also~~; alternatively, users may start their own parallel pool with a chosen number of cores). It then decomposes the full sequence of image pairs into sub-sequences~~the size of~~, each containing a number of image pairs equal to the number of cores. Finally, ~~it distributes~~ displacements are calculated in parallel on the image pairs within each sub-sequence ~~across the cores~~ (each on a different core in the computer~~to be computed in parallel~~). Figure 3 shows the increase in computation speed with number of cores used in different scenarios. This enables large datasets to be processed more rapidly, even on standard laptop and desktop computers.

185 2.2.3 Single- and multi-pass approaches

Displacements may be derived from an image pair either with a single pass across the images, or with multiple passes with gradually reducing window sizes (Thielicke and Stamhuis, 2014; Raffel et al., 2018). Single-pass methods generally have the advantage of generally being faster at coarse resolutions and are less at risk of smearing one erroneous value over a larger area. Multi-pass methods update displacement estimates over multiple iterations, refining initial coarse-window-size displacement calculations using progressively smaller window sizes. Multi-pass methods combine the advantages of better feature matching at large window sizes with the higher spatial resolution of small window sizes. Both methods are integrated into GIV, with a single-pass method based on ImGRAFT (Messerli and Grinsted, 2015) and a 3-iteration multi-pass algorithm modified from MatPIV (Sveen, 2004). Both functions have been tested in a number of previous studies, with MatPIV being used extensively in fluid-dynamics research (e.g., Sveen and Cowen, 2004; Sveen, 2004; Lee et al., 2017; Oertel and Süfke, 2020).
195 An experiment evaluating the difference between a normalized cross correlation algorithm and the multi-pass frequency domain cross correlation in GIV is given in the supplementary material. We find that the multi-pass frequency domain algorithm produces velocity maps with higher signal to noise ratio than the normalized cross correlation algorithm across test scenarios with a range of cloud cover.

2.2.4 Non-consecutive images

200 GIV may also calculate velocity maps for pairs of non-consecutive images, which we refer to as "temporal oversampling", resulting in much larger final datasets. The user inputs maximum and minimum temporal separations for image pairs, and GIV extracts all suitable pairs, including those that are not consecutive. For a dataset of n images, this theoretically enables a total of $(n^2 - n)/2$ image pairs. (~~For example, this would produce 19,900 image pairs from a 200-satellite-image time-series~~). For heavily clouded datasets this also has the advantage of increasing the likelihood of forming cloud-free image pairs.

205 2.2.5 Velocity map filtering and improvement

Apart from some scenarios and positions such as surges, spring speedups, and the margins of ice streams, glacier velocity gradients vary gradually in both space (low lateral velocity gradients) and time (low acceleration). Therefore, the accuracy of individual velocity measurements can be evaluated by comparing them to their immediate neighbours in both space and

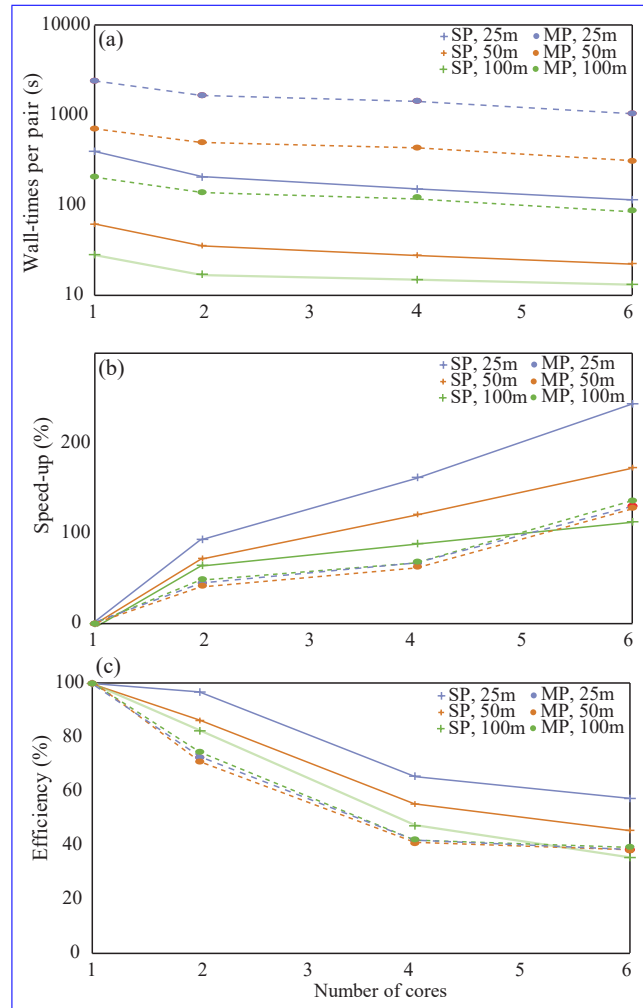


Figure 3. MP = Multi-pass; SP = Single-pass. Test conducted on a 12-image dataset of 10-m resolution, 1.7 million pixel images of Amalia Glacier, Chile using a Dell XPS 15 laptop (2×16GB DDR4 2666 MHz memory, 6-core Intel i7-8750H 2.20 GHz processor). In all cases, parallelization decreases runtime, and going from one to two cores improves runtime by 1.4–1.9×. Fine-resolution multi-pass runs usually yield the best velocity fields, and (b) shows that these benefit from the largest speed-up when parallelised.

time. Sudden jumps in space or time most likely represent erroneous velocities due to mismatches within the feature-tracking algorithm. This property is used in the GIV toolbox to improve the final velocity maps through the following workflow:

Firstly, GIV filters each individual velocity map through user-prescribed limits on velocity and flow direction, as well as outlier detection functions. This finds values that differ by more than 50% from their immediate neighbours (4 surrounding cells) and 200% from the mean of their larger local area (25 surrounding cells), removes these outlier values, and interpolates across these now-empty pixels using the remaining values. Secondly, GIV calculates the mean, standard deviation, median, minimum, and maximum velocities through time at each grid cell in the dataset. It then compares each individual value to

the mean value at that location for the entire dataset. Any values more than 1.5 standard deviations away from this mean are considered outliers. This process is carried out ~~both for the velocity for the x- and y- components of velocity, flow-speed and~~ flow-direction grids, and only values within the threshold for ~~both all~~ velocity and flow direction components are conserved. This provides an additional check, as erroneous values are unlikely to coincidentally match both the velocity and flow direction.

220 Finally, the entire dataset may be smoothed and interpolated in space or time and space according to the user's choices. This allows missing values at one timestep to be linearly infilled from neighbouring times ~~if the dataset is smooth enough to allow it.~~ In addition, the displacement of each image pair may be normalized to the displacement of a user-defined stable ground mask to correct for systematic georeferencing errors.

2.2.6 Temporal resampling

225 Variable satellite repeat intervals and the exclusion of entirely clouded or otherwise unusable images lead to unevenly spaced velocity timeseries that are more difficult to interpret. In order to reduce this challenge, GIV includes a function that automatically averages the data and re-samples it to monthly intervals. This is easy when all individual velocity maps cover periods of less than one month and do not overlap between months, but becomes more complex when they do. In many cases, image pairs with the shortest lag times (<7–10 days) are excluded because displacement over such a short time may be obscured by

230 offsets due to distortion and/or georeferencing errors. For the slowest-moving glaciers, this lower bound may be extended to several weeks or months. Lag times as long as the available imagery time series may be used so long as the surface of the glacier retains coherence in the image pairs.

GIV can determine monthly values by averaging across all image pairs that overlap with a given month. However, this produces an artificially smoothed dataset due to the influence of velocities measured across the boundaries of months. In order

235 to make use of longer lag-time pairs, we develop an iterative strategy for calculating monthly values. In the first place, GIV takes a weighted mean of all velocities covering that month to make an initial guess at monthly velocities. The weighting parameter is determined by the proportion of the individual map contained within ~~the given month, so for instance~~ a given month. For instance, a velocity entirely within one month will be weighted ~~1 and one,~~ while a velocity spread evenly over four months will be weighted 0.25. This initial estimate is then used to iterate between monthly averages and raw data values, with raw values

240 covering more than one month split into monthly values by subtracting the previous iteration's estimate of monthly averages from them (Figure 4). This procedure may extract average monthly velocities even for months lacking any data images. Outlier detection and maximum velocity filters are implemented ~~to prevent small errors based on used-provided maximum velocity and comparison to neighboring pixels. This prevents noise~~ in the raw data from being accentuated by the iterations, but ~~this~~ may also lead to loss of data if too large a proportion of the initial dataset is inaccurate. Due to this limitation, the iterative

245 calculations are not ~~be~~ adapted for some noisy datasets, in which the partial loss of temporal resolution by ~~simple-weighted~~ averaging will be preferable. Monthly averaging is performed as a post-processing step, and so may be repeated without the need to recalculate any raw velocity maps. Time series may also be generated from the raw data if monthly averaging is not desirable.

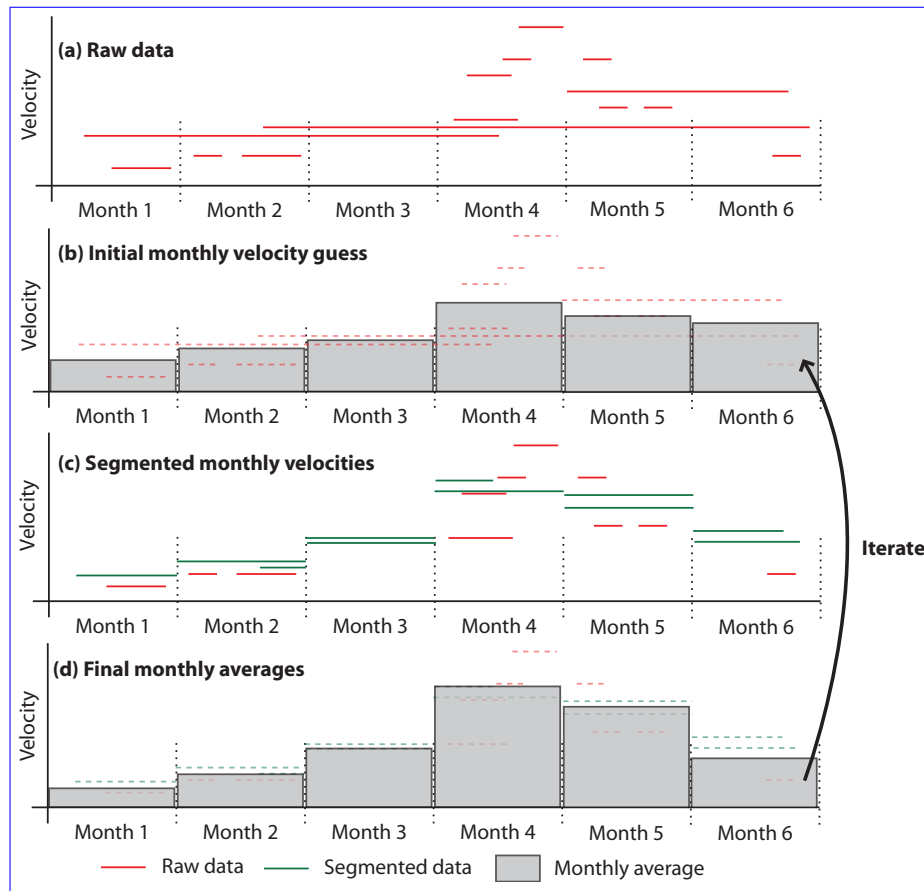


Figure 4. Schematic description of the techniques used to derive monthly velocities. The raw data (a) are combined in a weighted average to make an initial guess of monthly averages (b). The monthly averages are then used to segment longer time period velocity maps into their different monthly contributions (c). These are used to recalculate the monthly averages (d). Finally, GIV iterates over steps b–d for a number of times (e.g. 10) provided by user inputs. Note that an estimate may be made for the average velocity in ‘Month 3’, despite this month having no imagery available.

2.2.7 Georeferencing and plotting

250 As a final step, GIV will automatically georeference the velocity grids and save .geotiff files to the user’s computer. The toolbox also contains mapping tools that allow automatic generation of publication-quality images of the velocity and flow-direction maps (figure 5). Flow direction maps are plotted with a circular colormap, and all color maps used are color-blind friendly based on Crameri et al. (2020) and may be modified according to user preferences. In the following section we will examine some case studies of real glaciers and scenarios for which this model may be useful.

Ice-velocity measurements supply essential information for studies of glacier dynamics, thickness, subglacial hydrology, and mass balance. With its GUI-based inputs and potential for parallelization, GIV can calculate a monthly velocity field for any glacier around the world with only a few hours of work. As such, it may also be run alongside field-based expeditions in order to understand the current conditions of the glacier and aid in instrumentation positioning.

260 We present four case studies. The first is of Glaciar Perito Moreno (50.48°S, 73.11°W), where we use GIV to determine the displacement of automated ablation stakes in conjunction with fieldwork in Spring 2020. The second is Glacier d'Argentiére (45.95°N, 06.97°E), a small and well-studied valley glacier located in the French Alps. The third is ~~the Vavilov ice cap~~ Vavilov Ice Cap (79.32°N, 94.34°E), located on October Revolution Island, in the Arctic Ocean off the mainland Russian coast, whose western outlet glacier is now surging ~~into the ocean~~. Here we ~~validate~~ evaluate GIV against published results (Zheng et al., 265 2019b) using another image-based ice-velocity tool, CARST (Zheng et al., 2019a). Finally, we compute ice-flow velocities across the ~~Chimborazo ice cap~~ glaciers on Volcán Chimborazo (01.45°S, 78.82°W) in Ecuador.

3.1 Field-campaign support: Glaciar Perito Moreno and the Southern Patagonian Icefield

A team from the University of Minnesota installed ~~3~~ three automated weather stations and ~~3~~ three automated ablation stakes near the southern flank of Glaciar Perito Moreno in order to better understand the local conditions of this glacier and construct 270 temperature-index and energy-balance models for glacier ablation. We installed the automated ablation stakes, based ~~off of~~ on designs by Wickert (2014) and Wickert et al. (2019), and tested by Saberi et al. (2019) and Armstrong and Anderson (2020), for 20 days between the 23rd of February and 14th of March, 2020. In ~~slowly flowing~~ slow moving glaciers, ice flow may be largely neglected when considering equipment recovery. In rapidly flowing glaciers such as Perito Moreno, however, it may be relevant to consider the movement of the glacier when planning equipment recovery. This is particularly relevant where intense 275 crevassing makes both access and visibility difficult. Figure 6 shows how different positioning decisions may influence ease of recovery: ablation stakes installed in position PM1 will move tens of metres towards the glacier calving front in less than a month, whereas stakes in position PM3 will move less than 5 m towards the glacier flank. In our survey, stakes were installed around position PM3 for ease of access.

Figure 6 (b) also presents the case of Glaciar Europa, which drains the adjacent portion of the Southern Patagonian Icefield 280 in Chile. We also derived the mean velocity field of this glacier over the past 3 years using Sentinel-2 imagery (195 image pairs). GIV velocity measurements reveal that the central portion of Glaciar Europa at its outlet flows nearly 10,000 m/yr. If an ablation stake were installed in this area (point EU1), it would be displaced almost half a kilometre over the course of a 20-day survey. If it were instead placed at an alternative location 1 km to the West (EU2) it will be displaced only 20 metres in the same time period. This is an extreme case and the flow speeds of most glaciers are orders of magnitude slower, but showcases 285 the potential ~~value of deriving importance of deriving glacier surface~~ velocity fields for the success of a glaciological field campaign.

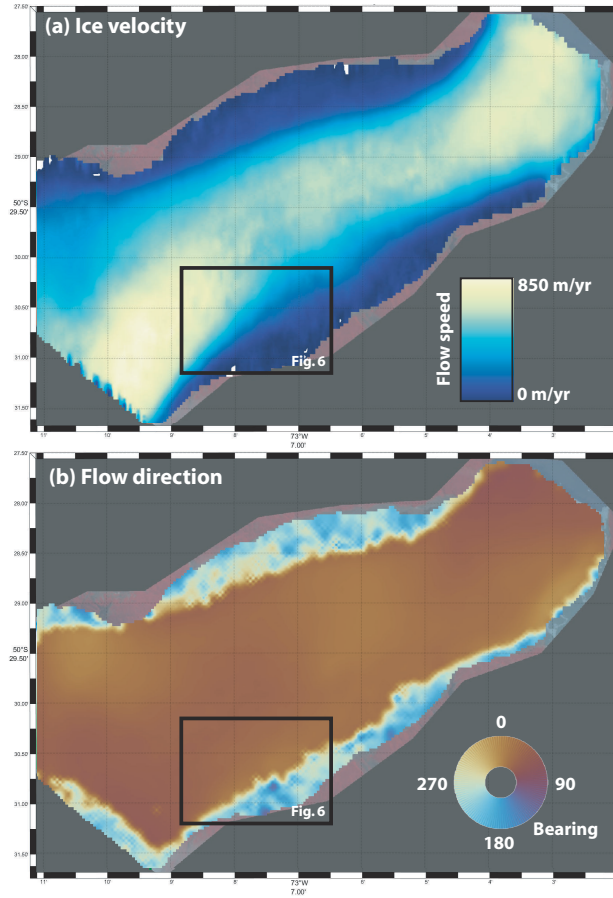


Figure 5. Mean flow velocity (m per year) (a) and direction (degrees) (b) of Glaciar Perito Moreno, Argentina for the first three months of 2020. Figure panels automatically generated from GIV, labels have been added and the color bars moved.

3.2 Valley-glacier velocity distribution: Glacier d’Argentière

In order to evaluate the effectiveness of GIV on smaller glaciers, we calculate a velocity field for a well-studied valley glacier in the Mont Blanc massif, Glacier d’Argentière (Benoit et al., 2015). We download one year worth of Sentinel-2 data (March 2019 – March 2020), containing over 1000 image pairs. These images are then used to derive a 25-m resolution mean-ice-velocity map, shown in Figure 7. The sparsity of features transverse to flow direction on Glacier d’Argentière make it difficult for feature-tracking methods to calculate velocities. Nevertheless, the resulting flow-velocity map is comparable to those derived using a SPOT satellite image pair from 2003 (Berthier et al., 2005; Rabatel et al., 2018), SAR and ground based photogrammetry (Benoit et al., 2015), and a different feature-tracking routine based on a modified version of ampcor (Millan et al., 2019). The velocity map highlights accelerated ice flow at the terminus icefall and on the steep tributary glacier to the SW of the main trunk (Figure 7). Main-trunk velocities are on the order of 45–70 m/yr, slightly slower than Berthier et al. (2005)’s SPOT

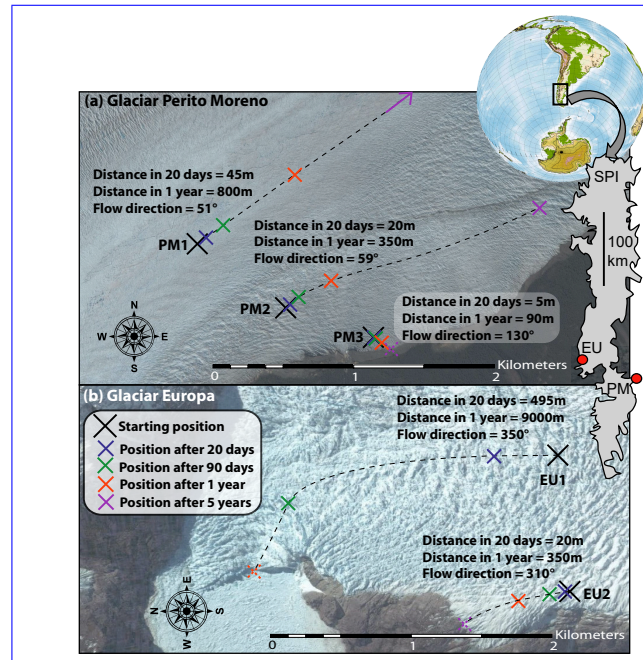


Figure 6. (a) Position of a point on Glaciar Perito Moreno (PM) with time for three different starting locations within 2 km of the glacier's southern margin. At PM1, ice speeds reach 800 m/yr and any equipment will be rapidly displaced. At PM3 ice-flow speeds are < 100 m per year and oriented towards the valley edge. (b) Identical plot for two points on Glaciar Europa (EU). Any equipment installed at EU1 will be displaced several kilometres and lost to calving in less than 6 months. [The inset shows an outline of the Southern Patagonian Icefield \(SPI\), with the locations of the two glaciers.](#) Imagery © Google Earth.

values but in line with Benoit et al. (2015)'s values. Our values represent the mean over an entire year, including the slower winter velocities [not](#) captured by Berthier et al. (2005). It is also possible that glacier thinning has reduced its flow velocity, but our data is not sufficient to evaluate this.

300 3.3 ~~Validating GIV by observing~~ Vavilov ~~ice-cap~~ Ice Cap dynamics

3.3.1 ~~Mapping ice surge~~

Arctic land-ice melt, [including both the Greenland Ice Sheet and all Arctic glaciers,](#) has contributed more than 20 mm to global sea level rise since the 1970s (Box et al., 2018). Most of these large glaciers ~~and ice-caps~~ remain remote and difficult to access, and high spatial and temporal resolution surface velocity maps provide one important tool to assess their response to changing environmental conditions.

Vavilov ~~ice-cap~~ Ice Cap is a 1700 km³ ~~ice-cap located~~ glacier on October Revolution Island in the Severnaya Zemlya archipelago, located in the Russian high arctic (Bassford et al., 2006). Until the 2010s, Vavilov ~~ice-cap~~ Ice Cap exhibited surface velocities of only a few tens of metres per year, typical of many cold-based high-arctic ice masses. In 2013, a large

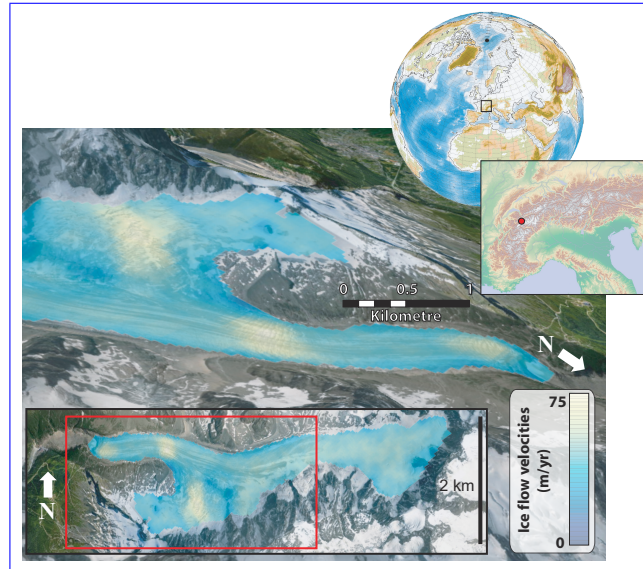


Figure 7. Perspective view of mean flow velocities of Glacier d'Argentière, France over the period 03/2019–03/2020. Imagery © Google Earth, scale for near margin of glacier.

portion of the marine-terminating western flank surged, with the ice front reaching more than 10 km beyond its prior ground-
 310 ing line by 2016 (Willis et al., 2018; Zheng et al., 2019b). This sudden shift in ice behaviour was not accompanied by any
 dramatic climatic shift, and the exact triggers are a matter of active debate (Willis et al., 2018, and references therein). Willis
 et al. (2018) proposed that the dramatic acceleration is related to the [ice-cap glacier](#) overriding weak marine sediments in
 the Kara Sea, which can deform easily and substantially increase ice velocity. The [ice-cap glacier](#) margin is also no longer
 frozen to bedrock, leading to associated removal of resistive stresses at the ice front (Willis et al., 2018). Rapid ice flow ini-
 315 tiates a set of internal feedbacks to further increase ice velocity, including strain softening of the ice itself; shear heating that
 produces meltwater, capable of reducing the effective normal stress of the ice and hence its friction against the bed; and po-
 tential infiltration of this water into the bed material, increasing its deformability ([Willis et al., 2018, and references therein](#))
[\(Sevestre and Benn, 2015; Willis et al., 2018, and references therein\)](#). With no direct data on subglacial conditions prior to or
 during the surge, the exact processes involved remain difficult to determine. We may, however, monitor surface ice velocities
 320 to examine the ongoing changes in ice kinematics.

[Visible-band Optical satellite](#) imagery from Vavilov [ice-cap Ice Cap](#) is available only for summer months (March to Septem-
 ber) due to darkness during the high-latitude boreal winter. We use GIV to derive a 100-m resolution ice-velocity map of a
 365-km² area of the Western flank of the [ice-cap using the entire glacier using all](#) Sentinel-2 [archive \(beginning in imagery](#)
[from 2016 \)-to 2020](#). Figure 8 (a) and (b) present two average yearly velocity maps for the apex of the [surges surge](#) in 2016 [and](#)
 325 [, and in](#) 2019. Panels (d) and (e) present timeseries of monthly velocities over the period from March 2016 to March 2020 at
 the locations shown in figure 8(c).

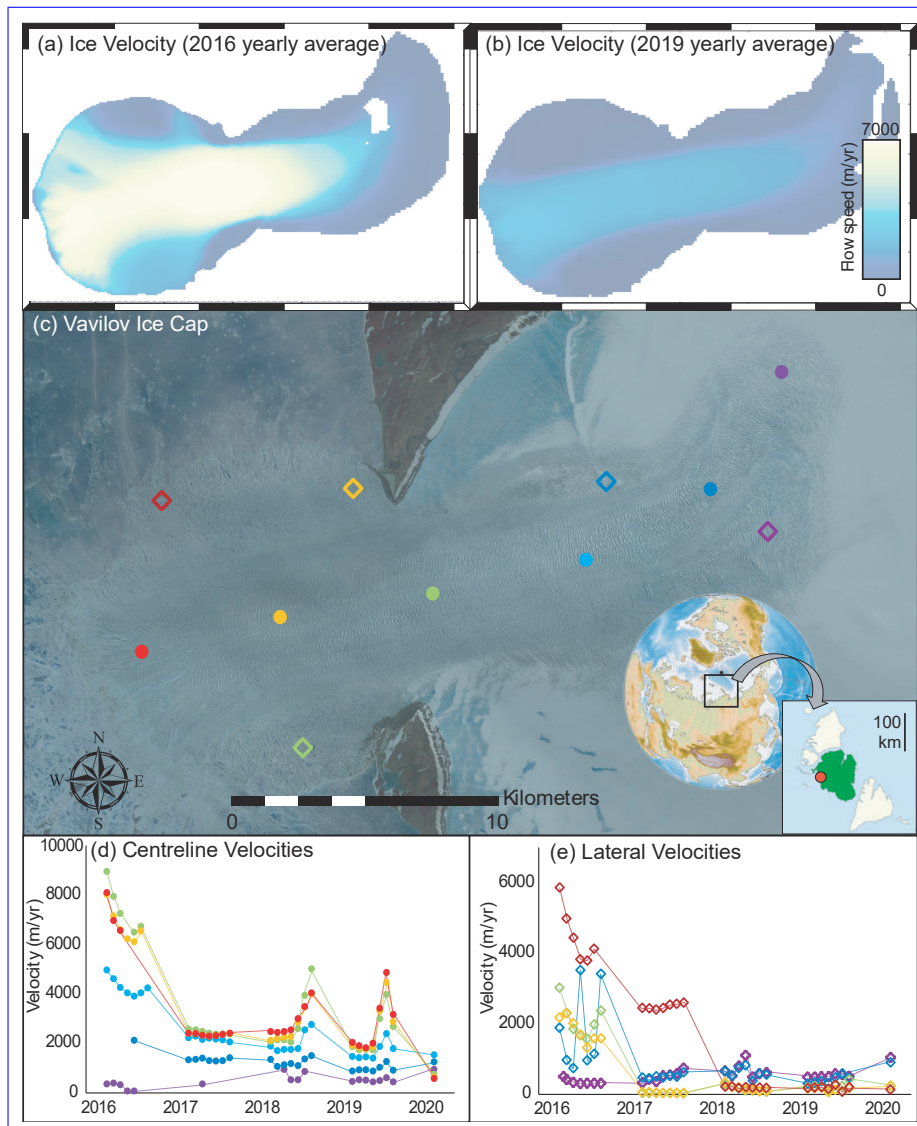


Figure 8. (a) and (b) ~~present~~ 100-m-resolution annual mean velocities for the western outlet glacier of Vavilov ~~ice cap~~ Ice Cap. (c) ~~displays~~ a 2019 Sentinel-2 image showing the main features of this outlet and the locations used to derive monthly timeseries. (d) and (e) ~~present~~ monthly resolution velocity timeseries along the glacier centreline and flanks using Sentinel-2 imagery.

Velocities of the centreline points converge over the time period considered: Although the velocities near the ice front decrease from the 2016 peak (red, orange, and green circles), velocities of regions most distant from the coast show a steady increase (purple points). The central portion of this newly formed outlet glacier shows distinct late-summer accelerations in both 2018 and 2019, reaching around double its spring and early summer rates and rapidly decaying (figure 7(d)). Within the newly formed western frontal lobe, extruded beyond the prior grounding line, flow has concentrated into a single branch with

well-developed shear margins separating a central region with rapid ice flow from slow-moving lateral portions of the glacier (Zheng et al., 2019b).

Extraction of high-resolution ice velocities in this region using GIV confirms Willis et al. (2018) and Zheng et al. (2019b)'s findings that the western portion of Vavilov has entered into a new fast-flow regime. The late summer velocity peaks in both 2018 and 2019 may shed some light on the driving forces behind this acceleration if associated ~~changed~~ changes in climatic, ice surface or ice basal conditions are identified. Ongoing monitoring will help to determine whether a similar peak occurs in ~~2020 or any following~~ subsequent years, and can be performed in near real time using GIV.

3.3.1 ~~Method validation~~

We compare our GIV-derived results against a velocity map of the front of the western outlet glacier generated by Zheng et al. (2019b) using CARST (Zheng et al., 2019a). Zheng et al. (2019b) generated their velocity map based on a single Landsat 8 pair dated 2017/05/06 and 2017/05/22. We compared the ice-surface velocity magnitude calculated from this pair to the May 2017 average velocity map generated from Sentinel-2 imagery using GIV through the approach described above. We georeferenced the two velocity maps using the glacier margins and other notable features. The difference map (Fig. 9(a)) displays the highest amplitude anomalies along the margins of the central high-velocity band. Differences between the GIV- and CARST-derived velocity maps are normally distributed, with a mean difference of -16 m per year (Fig 9(c)). This mean difference is $\leq 1\%$ the speed across the majority of the glacier surface (Fig 9(b)). In this region of the glacier surface, the annual variability in ice-surface velocities is on the order of several hundred metres per year (Fig 8(d) and (e)), and this difference may result from the slightly different dates covered or differing image resolutions (10 m for Sentinel-2 compared to 15–30 m for Landsat). The high-magnitude difference bands on either side of the fast-moving central region may also result in whole or part from georeferencing errors in GIV, in CARST, or in our work to georeference these two velocity maps to one another.

3.4 Ice-velocity of a small tropical ~~ice cap~~ glacier: Chimborazo

Many tropical glaciers ~~and ice caps~~ have limited to no ice-flow data from direct field measurements (Thompson et al., 2011). These are important water sources to millions of people (Bury et al., 2011; Chevallier et al., 2011; La Frenierre and Mark, 2017). Vergara et al. (2007) estimated the economic cost of glacier retreat on water use to be in the hundreds of millions of U.S. dollars, and the impact on Peru's electrical utility to be ~ 1.5 billion. High resolution estimates of ice velocity provide information on glacier state, and can contribute to practical decision making in the tropical Andes.

Chimborazo is a 6268 m high stratovolcano in Ecuador ~~eapped with an ice cap and~~ covered with 17 ~~outlet~~ glaciers. On Chimborazo's north-eastern flank, glacier meltwater drives nearly all of the discharge variability, and the disappearance of the prominent Reschreiter Glacier could decrease the discharge of the watershed's outlet stream by up to 50% (Sabeti et al., 2019). Due to its high elevation and steep slopes that are unstable in regions of recent ice retreat, the glaciers on Chimborazo are difficult to survey (Sabeti et al., 2019). No field measurements of glacier surface velocity have been conducted.

Chimborazo poses challenges to feature-tracking-based ice velocimetry, as its glaciers are small, regularly feature-poor or snow-covered, very slow moving, and cloud covered for large parts of the year. The velocity limitations are mitigated by using

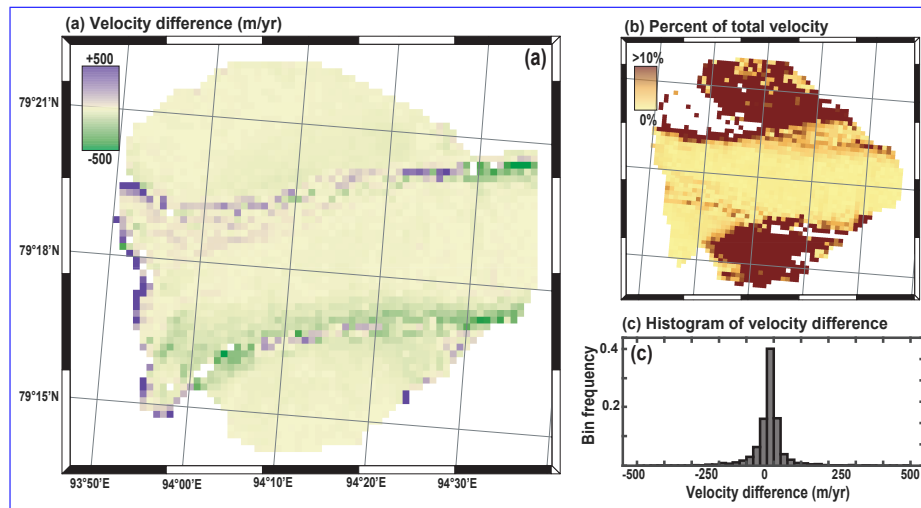


Figure 9. Comparison between Zheng et al. (2019b)'s velocity maps for Vavilov ~~ice cap~~ Ice Cap (Pair037_20170506_20170522) with results from GIV (May 2017 average). a) ~~shows a difference~~ Difference map, corresponding to Zheng et al. velocity minus GIV velocity, b) ~~shows what~~ percentage of the total velocity this difference represents (absolute value of the difference shown in a) divided by GIV velocity), and c) ~~is a~~ histogram of the difference values. The mean difference between the two velocity maps is less than 20 m per year, or less than 1% of the total velocity for much of the area.

only images with large temporal separation (acquisition dates more than six months apart). GIV is also well suited for extracting velocities from partially clouded imagery. We run GIV on the full Sentinel-2 dataset, which comprises of 91 individual partially or fully cloud-free images. These were cropped to Chimborazo, resulting in 3062 image pairs separated by at least six months. Resultant ice velocities for each pair were corrected for the mean displacement of a stable, non-glaciated region surrounding the ~~ice cap~~ glaciers. Results are shown in Figure 10. ~~The runtime for this calculation is approximately 2 hours on a Dell XPS 15 laptop (2×16GB DDR4 2666 MHz memory, 6-core Intel i7-8750H 2.20 GHz processor).~~

4 Discussion and Conclusions

These four examples underline GIV's flexibility, ease of use, and ability to rapidly process large datasets for calculating ice velocities in a range of environments. Most regular laptop and desktop computers now include at least 4 cores, which GIV uses to speed up calculations by a factor of two or more (Figure 3). This makes velocity-field calculations with hundreds to ~~tens of~~ thousands of image pairs practical on regular computers. The inclusion of 'temporal oversampling' allows much larger datasets to be generated than via simple consecutive-image comparison; a dataset of 100 images may in fact include several thousand usable image pairs. We combine methodological advances in feature tracking and image processing from both geoscience and engineering toolboxes, and develop new filtering techniques to improve the quality of the final surface-velocity maps. GIV

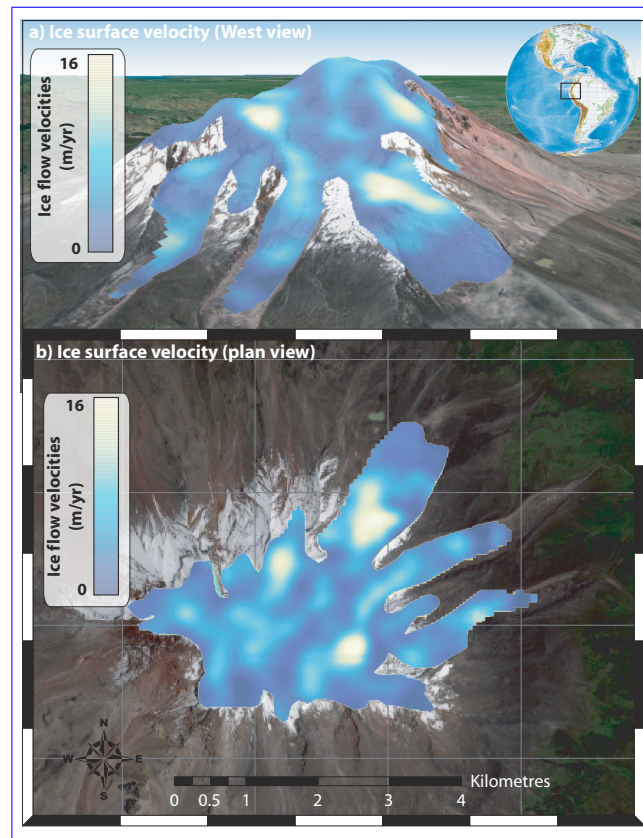


Figure 10. Ice-surface-velocity map for the Chimborazo glaciers calculated with GIV. Imagery © Google Earth and Sentinel-2.

provides a rapid and easy-to-use interface (shown in Figure 11) and a user manual, and may also be of use to communities who would not generally be involved with glacier remote sensing (Van Wyk de Vries, 2020a, b)(??).

Main graphical user interface for GIV, showing the main input fields. This interface may either be run through MATLAB or as an independent desktop app with no licensing requirements.

Many other feature-tracking algorithms have been used in glaciological research. These include CARST (Cryosphere and Remote Sensing), COSI-corr (Co-registration of Optically Sensed Images and Correlation: Leprince et al., 2007b), AutoRIFT (Autonomous Repeat Image), ImGRAFT (Image Georectification and Feature Tracking: Messerli and Grinsted, 2015), and SenDiT (the Sentinel-2 Displacement Tool). CARST contains a mixture of Python and Bash scripts used to monitor changes in glaciers, and includes feature-tracking and ice-elevation-change-monitoring tools (Willis et al., 2018; Zheng et al., 2018, 2019a). COSI-Corr is a flexible co-registration and feature-tracking tool written in IDL, implemented in the ENVI GIS package, and initially used for measuring co-seismic deformation. Auto-RIFT is a Python-based feature-tracking algorithm (Gardner et al., 2018) with similar core components to GIV. It was used to calculate yearly-resolution average velocity maps of the Antarctic and Greenland ice sheets (ITS_LIVE dataset). ImGRAFT is a MATLAB-based toolbox for georectifying and feature-tracking of ground-based imagery, and may

Figure 11. ~~Ice-surface-velocity-map~~ Main graphical user interface for GIV, showing the ~~Chimborazo-ice-cap-calculated-main~~ input fields. This interface may either be run through MATLAB or as an independent desktop app with GIV no licensing requirements. Imagery © Google Earth and Sentinel-2.

also be used on satellite imagery. SenDiT provides a platform to automatically download and generate velocity maps based on Sentinel-2 data, using a Python interface with bindings to the C- and Fortran-based *imcorr* toolbox (Scambos et al., 1992) for feature-tracking calculations.

395 In some circumstances, GIV will not be the most suitable feature tracking tool. For example, users who need to manually perform prior image co-registration (e.g. with airphotos) may wish to the built-in workflow in COSI-Corr. The objective of GIV is not to compete with or replace all the above tools, but rather to provide an easy-to-use, flexible, and robust alternative. GIV is GIV is easily learned and is not computationally time-consuming, and the results derived with it are easy to reproduce.

GIV allows users to modify image-processing and feature-tracking parameters based on their expert knowledge of particular glaciers, without the need for specific computational knowledge. GIV may be run either directly through MATLAB functions, through a MATLAB graphical user interface (~~Van Wyk de Vries, 2020a~~), or as an independent desktop app that may be run with no MATLAB license (~~Van Wyk de Vries, 2020b~~). GIV has been tested and successfully run on Windows, Mac and Linux operating systems.

In summary, GIV is a versatile, GUI-based, and fully parallelised toolbox that enables rapid calculation of glacier velocity fields from satellite imagery. GIV builds upon recent improvements in optical satellite imagery availability and resolution to extract high temporal and spatial resolution velocity maps, and uses novel and pre-existing filters to optimise the quality of these velocity maps. GIV has been successfully tested on a wide range of environments, including small valley glaciers (Glacier d'Argentière, France), tropical ~~ice-caps~~ glaciers (Volcán Chimborazo, Ecuador), and large outlet glaciers (Glacier Perito Moreno, Argentina, and outflow from ~~the~~ Vavilov Ice Cap, Russia). We show that ice-velocity datasets are versatile and may be used to compliment field campaigns, and study the dynamics of large and small glaciers. Source code and pre-compiled binary executables for GIV are available from ~~Van Wyk de Vries (2020a)~~ and ~~Van Wyk de Vries (2020b)~~ and ?.

Code availability. MATLAB code for GIV may be downloaded from <https://github.com/MaxVWDV/glacier-image-velocimetry> (?). The GIV standalone app may be downloaded from <https://github.com/MaxVWDV/glacier-image-velocimetry-app> (?). Both include a user manual and an example dataset.

Author contributions. MV and AW planned the project. MV wrote the code and ran the examples. MV and AW wrote and edited the manuscript.

Competing interests. The authors declare no competing interests.

Acknowledgements. MV was supported by a University of Minnesota College of Science and Engineering fellowship. Ben Popken assisted with early testing of GIV. Emi Ito, Kelly MacGregor, Jeff La Frenierre, Matias Romero, Shanti B. Penprase, Jabari Jones and Kerry L. Callaghan provided comments on this manuscript. ~~We thank~~ David Carchipulla helped improve image-download workflows. Conversations about feature tracking with Whyjay Zheng, Shashank Bhushan, Will Kochtitzky, and David Shean have helped refine the ideas in this paper and in GIV's code. We acknowledge Ted Scambos and two anonymous ~~reviewer~~ referees for thoughtful reviews, which improved both the manuscript and the associated toolbox. We further ~~acknowledge~~ thank editor Harry Zekollari for ~~providing welcome feedback and suggestions~~ detailed suggestions, which were valuable for fine-tuning our text and figures. This material is based upon work supported by the National Science Foundation under Grant No. EAR-1714614, coordinated by Lead PI Maria Beatrice Magnani.

References

- AghaKouchak, A., Farahmand, A., Melton, F. S., Teixeira, J., Anderson, M. C., Wardlow, B. D., and Hain, C. R.: Remote sensing of drought: Progress, challenges and opportunities, *Reviews of Geophysics*, 53, 452–480, <https://doi.org/10.1002/2014RG000456>, <http://agupubs.onlinelibrary.wiley.com/doi/abs/10.1002/2014RG000456>, _eprint: <https://onlinelibrary.wiley.com/doi/pdf/10.1002/2014RG000456>, 2015.
- Altena, B.: Observing change in glacier flow by using optical satellites, <https://www.duo.uio.no/handle/10852/61747>, accepted: 2018-05-28T11:09:27Z, 2018.
- Altena, B., Scambos, T., Fahnestock, M., and Kääb, A.: Extracting recent short-term glacier velocity evolution over southern Alaska and the Yukon from a large collection of Landsat data., *Cryosphere*, 13, 2019.
- Armstrong, W. H. and Anderson, R. S.: Ice-marginal lake hydrology and the seasonal dynamical evolution of Kennicott Glacier, Alaska, *Journal of Glaciology*, pp. 1–15, publisher: Cambridge University Press, 2020.
- Bakke, J. and Nesje, A.: Equilibrium-Line Altitude (ELA), in: *Encyclopedia of Snow, Ice and Glaciers*, edited by Singh, V. P., Singh, P., and Haritashya, U. K., pp. 268–277, Springer Netherlands, Dordrecht, https://doi.org/10.1007/978-90-481-2642-2_140, https://doi.org/10.1007/978-90-481-2642-2_140, 2011.
- Bamber, J. L. and Rivera, A.: A review of remote sensing methods for glacier mass balance determination, *Global and Planetary Change*, 59, 138–148, <https://doi.org/10.1016/j.gloplacha.2006.11.031>, <http://www.sciencedirect.com/science/article/pii/S0921818106003055>, 2007.
- Bassford, R. P., Siegert, M. J., Dowdeswell, J. A., Oerlemans, J., Glazovsky, A. F., and Macheret, Y. Y.: Quantifying the Mass Balance of Ice Caps on Severnaya Zemlya, Russian High Arctic. I: Climate and Mass Balance of the Vavilov Ice Cap, Arctic, Antarctic, and Alpine Research, 38, 1–12, [https://doi.org/10.1657/1523-0430\(2006\)038\[0001:QTMBOI\]2.0.CO;2](https://doi.org/10.1657/1523-0430(2006)038[0001:QTMBOI]2.0.CO;2), <https://www.tandfonline.com/doi/abs/10.1657/1523-0430%282006%29038%5B0001%3AQTMBOI%5D2.0.CO%3B2>, publisher: Taylor & Francis _eprint: <https://www.tandfonline.com/doi/pdf/10.1657/1523-0430%282006%29038%5B0001%3AQTMBOI%5D2.0.CO%3B2>, 2006.
- Benoit, L., Dehecq, A., Pham, H.-T., Vernier, F., Trouvé, E., Moreau, L., Martin, O., Thom, C., Pierrot-Deseilligny, M., and Briole, P.: Multi-method monitoring of Glacier d’Argentière dynamics, *Annals of Glaciology*, 56, 118–128, <https://doi.org/10.3189/2015AoG70A985>, https://www.cambridge.org/core/product/identifier/S0260305500250398/type/journal_article, 2015.
- Berthier, E., Vadon, H., Baratoux, D., Arnaud, Y., Vincent, C., Feigl, K. L., Rémy, F., and Legrésy, B.: Surface motion of mountain glaciers derived from satellite optical imagery, *Remote Sensing of Environment*, 95, 14–28, <https://doi.org/10.1016/j.rse.2004.11.005>, <http://www.sciencedirect.com/science/article/pii/S0034425704003463>, 2005.
- Bindschadler, R., Vornberger, P., Fleming, A., Fox, A., Mullins, J., Binnie, D., Paulsen, S. J., Granneman, B., and Gorodetzky, D.: The Landsat Image Mosaic of Antarctica, *Remote Sensing of Environment*, 112, 4214–4226, <https://doi.org/10.1016/j.rse.2008.07.006>, <http://www.sciencedirect.com/science/article/pii/S003442570800223X>, 2008.
- Bindschadler, R. A. and Scambos, T. A.: Satellite-Image-Derived Velocity Field of an Antarctic Ice Stream, *Science*, 252, 242–246, <https://doi.org/10.1126/science.252.5003.242>, <https://science.sciencemag.org/content/252/5003/242>, 1991.
- Bottomley, J. T.: Flow of Viscous Materials—A Model Glacier, *Nature*, 21, 159–159, <https://doi.org/10.1038/021159a0>, <http://www.nature.com/articles/021159a0>, number: 529 Publisher: Nature Publishing Group, 1879.
- Box, J. E., Colgan, W. T., Wouters, B., Burgess, D. O., O’Neel, S., Thomson, L. I., and Mernild, S. H.: Global sea-level contribution from Arctic land ice: 1971–2017, *Environmental Research Letters*, 13, 125 012, <https://doi.org/10.1088/1748-9326/aaf2ed>, <https://doi.org/10.1088%2F1748-9326%2Faaf2ed>, publisher: IOP Publishing, 2018.

- Buchhave, P.: Particle image velocimetry—status and trends, *Experimental Thermal and Fluid Science*, 5, 586–604, [https://doi.org/10.1016/0894-1777\(92\)90016-X](https://doi.org/10.1016/0894-1777(92)90016-X), <http://www.sciencedirect.com/science/article/pii/089417779290016X>, 1992.
- 465 Bury, J. T., Mark, B. G., McKenzie, J. M., French, A., Baraer, M., Huh, K. I., Zapata Luyo, M. A., and Gómez López, R. J.: Glacier recession and human vulnerability in the Yanamarey watershed of the Cordillera Blanca, Peru, *Climatic Change*, 105, 179–206, <https://doi.org/10.1007/s10584-010-9870-1>, <https://doi.org/10.1007/s10584-010-9870-1>, 2011.
- Chadwell, C. D.: Reliability analysis for design of stake networks to measure glacier surface velocity, *Journal of Glaciology*, 45, 154–164, <https://doi.org/10.3189/S0022143000003130>, <http://www.cambridge.org/core/journals/journal-of-glaciology/article/reliability-analysis-for-design-of-stake-networks-to-measure-glacier-surface-velocity/F342FD59DA4D2EA6689383D677351269>, publisher: Cambridge University Press, 1999.
- 470 Chevallier, P., Pouyaud, B., Suarez, W., and Condom, T.: Climate change threats to environment in the tropical Andes: glaciers and water resources, *Regional Environmental Change*, 11, 179–187, <https://doi.org/10.1007/s10113-010-0177-6>, <http://link.springer.com/10.1007/s10113-010-0177-6>, 2011.
- 475 Cramer, F., Shephard, G. E., and Heron, P. J.: The misuse of colour in science communication, *Nature Communications*, 11, 5444, <https://doi.org/10.1038/s41467-020-19160-7>, <http://www.nature.com/articles/s41467-020-19160-7>, 2020.
- Darji, S., Shah, R. D., Oza, S., and Bahuguna, I. M.: Inter-Comparison of Various Feature Tracking Tools Deriving Glacier Ice Velocity, 7, 8, 2018.
- Davies, B. J. and Glasser, N. F.: Accelerating shrinkage of Patagonian glaciers from the Little Ice Age (~AD 1870) to 2011, *Journal of Glaciology*, 58, 1063–1084, <https://doi.org/10.3189/2012JoG12J026>, <https://www.cambridge.org/core/journals/journal-of-glaciology/article/accelerating-shrinkage-of-patagonian-glaciers-from-the-little-ice-age-ad-1870-to-2011/933AF3AB94615A1E7AACF85510FF7FD1>, 2012.
- Deeley, R. M. and Parr, P. H.: XVI. The Hintereis Glacier, *The London, Edinburgh, and Dublin Philosophical Magazine and Journal of Science*, 27, 153–176, publisher: Taylor & Francis, 1914.
- 485 Drusch, M., Del Bello, U., Carlier, S., Colin, O., Fernandez, V., Gascon, F., Hoersch, B., Isola, C., Laberinti, P., Martimort, P., Meygret, A., Spoto, F., Sy, O., Marchese, F., and Bargellini, P.: Sentinel-2: ESA’s Optical High-Resolution Mission for GMES Operational Services, *Remote Sensing of Environment*, 120, 25–36, <https://doi.org/10.1016/j.rse.2011.11.026>, <http://www.sciencedirect.com/science/article/pii/S0034425712000636>, 2012.
- Earl, L. and Gardner, A.: A satellite-derived glacier inventory for North Asia, *Annals of Glaciology*, 57, 50–60, <https://doi.org/10.3189/2016AoG71A008>, <http://www.cambridge.org/core/journals/annals-of-glaciology/article/satellitederived-glacier-inventory-for-north-asia/9CFCE79604C90AECCCAA5E0308D91B93>, publisher: Cambridge University Press, 2016.
- Fahnestock, M., Scambos, T., Moon, T., Gardner, A., Haran, T., and Klinger, M.: Rapid large-area mapping of ice flow using Landsat 8, *Remote Sensing of Environment*, 185, 84–94, <https://doi.org/10.1016/j.rse.2015.11.023>, <http://www.sciencedirect.com/science/article/pii/S003442571530211X>, 2016.
- 495 Fitch, A., Kadyrov, A., Christmas, W., and Kittler, J.: Orientation Correlation, in: *Proceedings of the British Machine Vision Conference 2002*, pp. 11.1–11.10, British Machine Vision Association, Cardiff, <https://doi.org/10.5244/C.16.11>, <http://www.bmva.org/bmvc/2002/papers/95/index.html>, 2002.
- Forbes, J. D.: *The Glacier Theory*, google-Books-ID: wPoTAAAAQAAJ, 1840.

- 500 Forbes, J. D.: XII. Illustrations of the viscous theory of glacier motion. - Part I. Containing experiments on the flow of plastic bodies, and observations on the phenomena of lava streams, *Philosophical Transactions of the Royal Society of London*, 136, 143–155, <https://doi.org/10.1098/rstl.1846.0013>, <https://royalsocietypublishing.org/doi/abs/10.1098/rstl.1846.0013>, publisher: Royal Society, 1846.
- Fowler, A.: Weertman, Lliboutry and the development of sliding theory, *Journal of Glaciology*, 56, 965–972, <https://doi.org/10.3189/002214311796406112>, [https://www.cambridge.org/core/product/identifier/S0022143000213191/type/journal_](https://www.cambridge.org/core/product/identifier/S0022143000213191/type/journal_article)
- 505 article, 2010.
- Frigo, M. and Johnson, S.: FFTW: an adaptive software architecture for the FFT, in: *Proceedings of the 1998 IEEE International Conference on Acoustics, Speech and Signal Processing, ICASSP '98* (Cat. No.98CH36181), vol. 3, pp. 1381–1384, IEEE, Seattle, WA, USA, <https://doi.org/10.1109/ICASSP.1998.681704>, <http://ieeexplore.ieee.org/document/681704/>, 1998.
- Frigo, M. and Johnson, S.: The Design and Implementation of FFTW3, *Proceedings of the IEEE*, 93, 216–231, <https://doi.org/10.1109/JPROC.2004.840301>, conference Name: *Proceedings of the IEEE*, 2005.
- 510 Gardner, A., Fahnestock, M., and Scambos, T.: ITS_LIVE Regional Glacier and Ice Sheet Surface Velocities., doi:10.5067/6II6VW8LLWJ7, 2020.
- Gardner, A. S., Moholdt, G., Scambos, T., Fahnestock, M., Ligtenberg, S., Broeke, M. v. d., and Nilsson, J.: Increased West Antarctic and unchanged East Antarctic ice discharge over the last 7 years, *The Cryosphere*, 12, 521–547, [https://doi.org/https://doi.org/10.5194/tc-12-](https://doi.org/https://doi.org/10.5194/tc-12-521-2018)
- 515 521-2018, <https://www.the-cryosphere.net/12/521/2018/>, publisher: Copernicus GmbH, 2018.
- Grant, I.: Particle image velocimetry: A review, *Proceedings of the Institution of Mechanical Engineers, Part C: Journal of Mechanical Engineering Science*, 211, 55–76, <https://doi.org/10.1243/0954406971521665>, <https://doi.org/10.1243/0954406971521665>, publisher: IMECHE, 1997.
- Harris, A.: *Thermal Remote Sensing of Active Volcanoes: A User's Manual*, Cambridge University Press, google-Books-ID: xY4oYzbH0ooC, 2013.
- 520 Heid, T. and Kääb, A.: Evaluation of existing image matching methods for deriving glacier surface displacements globally from optical satellite imagery, *Remote Sensing of Environment*, 118, 339–355, <https://doi.org/10.1016/j.rse.2011.11.024>, <http://www.sciencedirect.com/science/article/pii/S0034425711004214>, 2012a.
- Heid, T. and Kääb, A.: Repeat optical satellite images reveal widespread and long term decrease in land-terminating glacier speeds, *The Cryosphere*, 6, 467–478, <https://doi.org/10.5194/tc-6-467-2012>, <https://www.the-cryosphere.net/6/467/2012/>, 2012b.
- 525 Hooke, R. L., Calla, P., Holmlund, P., Nilsson, M., and Stroeven, A.: A 3 Year Record of Seasonal Variations in Surface Velocity, Storglaciären, Sweden, *Journal of Glaciology*, 35, 235–247, <https://doi.org/10.3189/S0022143000004561>, <http://www.cambridge.org/core/journals/journal-of-glaciology/article/3-year-record-of-seasonal-variations-in-surface-velocity-storglaciaren-sweden/2BF67175ACC7E8843B2AC980C4804F4A>, publisher: Cambridge University Press, 1989.
- 530 How, P., Hulton, N. R. J., Buie, L., and Benn, D. I.: PyTrx: A Python-Based Monoscopic Terrestrial Photogrammetry Toolset for Glaciology, *Frontiers in Earth Science*, 8, <https://doi.org/10.3389/feart.2020.00021>, <https://www.frontiersin.org/articles/10.3389/feart.2020.00021/full>, publisher: Frontiers, 2020.
- Howat, I. M., Negrete, A., and Smith, B.: The Greenland Ice Mapping Project (GIMP) land classification and surface elevation data sets, <https://doi.org/10.5194/tc-8-1509-2014>, 2014.
- 535 Howat, I. M., Porter, C., Smith, B. E., Noh, M.-J., and Morin, P.: The Reference Elevation Model of Antarctica, *The Cryosphere*, 13, 665–674, <https://doi.org/https://doi.org/10.5194/tc-13-665-2019>, <https://tc.copernicus.org/articles/13/665/2019/>, publisher: Copernicus GmbH, 2019.

- Hui, F., Cheng, X., Liu, Y., Zhang, Y., Ye, Y., Wang, X., Li, Z., Wang, K., Zhan, Z., Guo, J., Huang, H., Li, X., Guo, Z., and Gong, P.: An improved Landsat Image Mosaic of Antarctica, *Science China Earth Sciences*, 56, 1–12, <https://doi.org/10.1007/s11430-012-4481-5>, 2013.
- James, M. R., How, P., and Wynn, P. M.: Pointcatcher software: analysis of glacial time-lapse photography and integration with multitemporal digital elevation models, *Journal of Glaciology*, 62, 159–169, <https://doi.org/10.1017/jog.2016.27>, <http://www.cambridge.org/core/journals/journal-of-glaciology/article/pointcatcher-software-analysis-of-glacial-timelapse-photography-and-integration-with-multitemporal-digital-elevation-models/23EC92804DE7C5EED7229D0ACE31D90B>, publisher: Cambridge University Press, 2016.
- Jawak, S. D., Kumar, S., Luis, A. J., Bartanwala, M., Tummala, S., and Pandey, A. C.: Evaluation of Geospatial Tools for Generating Accurate Glacier Velocity Maps from Optical Remote Sensing Data, *Proceedings*, 2, 341, <https://doi.org/10.3390/ecrs-2-05154>, <https://www.mdpi.com/2504-3900/2/7/341>, 2018.
- Kamb, B. and LaChapelle, E.: Direct Observation of the Mechanism of Glacier Sliding Over Bedrock*, *Journal of Glaciology*, 5, 159–172, <https://doi.org/10.3189/S0022143000028756>, <http://www.cambridge.org/core/journals/journal-of-glaciology/article/direct-observation-of-the-mechanism-of-glacier-sliding-over-bedrock/A032752BFEA9BB2628AC95966D72C332>, publisher: Cambridge University Press, 1964.
- Klemas, V. V.: The Role of Remote Sensing in Predicting and Determining Coastal Storm Impacts, *Journal of Coastal Research*, 25, 1264–1275, <https://doi.org/10.2112/08-1146.1>, [https://meridian.allenpress.com/jcr/article/25/6\(256\)/1264/28316/The-Role-of-Remote-Sensing-in-Predicting-and](https://meridian.allenpress.com/jcr/article/25/6(256)/1264/28316/The-Role-of-Remote-Sensing-in-Predicting-and), publisher: Allen Press, 2009.
- Kobayashi, T. and Otsu, N.: Image Feature Extraction Using Gradient Local Auto-Correlations, *Computer Vision - ECCV 2008*, 10th European Conference on Computer Vision, 2008.
- Kääb, A. and Vollmer, M.: Surface Geometry, Thickness Changes and Flow Fields on Creeping Mountain Permafrost: Automatic Extraction by Digital Image Analysis, *Permafrost and Periglacial Processes*, 11, 315–326, [https://doi.org/10.1002/1099-1530\(200012\)11:4<315::AID-PPP365>3.0.CO;2-J](https://doi.org/10.1002/1099-1530(200012)11:4<315::AID-PPP365>3.0.CO;2-J), <http://onlinelibrary.wiley.com/doi/abs/10.1002/1099-1530%28200012%2911%3A4%3C315%3A%3AAID-PPP365%3E3.0.CO%3B2-J>, [_eprint: https://onlinelibrary.wiley.com/doi/pdf/10.1002/1099-1530%28200012%2911%3A4%3C315%3A%3AAID-PPP365%3E3.0.CO%3B2-J](https://onlinelibrary.wiley.com/doi/pdf/10.1002/1099-1530%28200012%2911%3A4%3C315%3A%3AAID-PPP365%3E3.0.CO%3B2-J), 2000.
- Kääb, A., Winsvold, S. H., Altena, B., Nuth, C., Nagler, T., and Wuite, J.: Glacier Remote Sensing Using Sentinel-2. Part I: Radiometric and Geometric Performance, and Application to Ice Velocity, *Remote Sensing*, 8, 598, <https://doi.org/10.3390/rs8070598>, <https://www.mdpi.com/2072-4292/8/7/598>, number: 7 Publisher: Multidisciplinary Digital Publishing Institute, 2016.
- La Frenierre, J. and Mark, B. G.: Detecting Patterns of Climate Change at Volcán Chimborazo, Ecuador, by Integrating Instrumental Data, Public Observations, and Glacier Change Analysis, *Annals of the American Association of Geographers*, 107, 979–997, <https://doi.org/10.1080/24694452.2016.1270185>, <https://doi.org/10.1080/24694452.2016.1270185>, publisher: Taylor & Francis _eprint: <https://doi.org/10.1080/24694452.2016.1270185>, 2017.
- Lee, R. M., Yue, H., Rappel, W.-J., and Losert, W.: Data from: Inferring single cell behavior from large-scale epithelial sheet migration patterns, <https://doi.org/https://doi.org/10.13016/M2855R>, <http://drum.lib.umd.edu/handle/1903/19190>, accepted: 2017-04-12T17:46:08Z type: dataset, 2017.
- Leprieux, S., Ayoub, F., Klinger, Y., and Avouac, J.-P.: Co-Registration of Optically Sensed Images and Correlation (COSI-Corr): an operational methodology for ground deformation measurements, in: 2007 IEEE International Geoscience and Remote Sensing Symposium,

- 575 pp. 1943–1946, IEEE, Barcelona, Spain, <https://doi.org/10.1109/IGARSS.2007.4423207>, <http://ieeexplore.ieee.org/document/4423207/>, 2007a.
- Leprince, S., Barbot, S., Ayoub, F., and Avouac, J.-P.: Automatic and Precise Orthorectification, Coregistration, and Subpixel Correlation of Satellite Images, Application to Ground Deformation Measurements, *IEEE Transactions on Geoscience and Remote Sensing*, 45, 1529–1558, <https://doi.org/10.1109/TGRS.2006.888937>, 2007b.
- 580 Mair, D., Willis, I., Fischer, U. H., Hubbard, B., Nienow, P., and Hubbard, A.: Hydrological controls on patterns of surface, internal and basal motion during three “spring events”: Haut Glacier d’Arolla, Switzerland, *Journal of Glaciology*, 49, 555–567, <https://doi.org/10.3189/172756503781830467>, <http://www.cambridge.org/core/journals/journal-of-glaciology/article/hydrological-controls-on-patterns-of-surface-internal-and-basal-motion-during-three-spring-events-haut-glacier-darolla-switzerland/9C10F4D8C42938F396AEF8E372F55247>, publisher: Cambridge University Press, 2003.
- 585 Marc, O. and Hovius, N.: Amalgamation in landslide maps: effects and automatic detection, *Natural Hazards and Earth System Sciences*, 15, 723–733, <https://doi.org/https://doi.org/10.5194/nhess-15-723-2015>, <https://www.nat-hazards-earth-syst-sci.net/15/723/2015/nhess-15-723-2015.html>, publisher: Copernicus GmbH, 2015.
- Meier, M. F. and Tangborn, W. V.: Net Budget and Flow of South Cascade Glacier, Washington, *Journal of Glaciology*, 5, 547–566, <https://doi.org/10.3189/S0022143000018608>, <http://www.cambridge.org/core/journals/journal-of-glaciology/article/net-budget-and-flow-of-south-cascade-glacier-washington/440E67FA2A6041F58689DDBB65733502>, publisher: Cambridge University Press, 1965.
- 590 Messerli, A. and Grinsted, A.: Image georectification and feature tracking toolbox: ImGRAFT, *Geoscientific Instrumentation, Methods and Data Systems*, 4, 23–34, <https://doi.org/10.5194/gi-4-23-2015>, <https://www.geosci-instrum-method-data-syst.net/4/23/2015/>, 2015.
- Metternicht, G., Hurni, L., and Gogu, R.: Remote sensing of landslides: An analysis of the potential contribution to geo-spatial systems for hazard assessment in mountainous environments, *Remote Sensing of Environment*, 98, 284–303, <https://doi.org/10.1016/j.rse.2005.08.004>, <http://www.sciencedirect.com/science/article/pii/S0034425705002506>, 2005.
- 595 Millan, R.: Ice thickness and bed elevation of the Patagonian Icefields, <https://doi.org/10.7280/d11q17>, <https://dash.lib.uci.edu/stash/dataset/doi:10.7280/D11Q17>, type: dataset, 2019.
- Millan, R., Mouginot, J., Rabatel, A., Jeong, S., Cusicanqui, D., Derkacheva, A., and Chekki, M.: Mapping Surface Flow Velocity of Glaciers at Regional Scale Using a Multiple Sensors Approach, *Remote Sensing*, 11, 2498, <https://doi.org/10.3390/rs11212498>, <https://www.mdpi.com/2072-4292/11/21/2498>, number: 21 Publisher: Multidisciplinary Digital Publishing Institute, 2019.
- 600 Minchew, B. M., Simons, M., Riel, B., and Milillo, P.: Tidally induced variations in vertical and horizontal motion on Rutford Ice Stream, West Antarctica, inferred from remotely sensed observations, *Journal of Geophysical Research: Earth Surface*, 122, 167–190, <https://doi.org/10.1002/2016JF003971>, <http://agupubs.onlinelibrary.wiley.com/doi/abs/10.1002/2016JF003971>, _eprint: <https://onlinelibrary.wiley.com/doi/pdf/10.1002/2016JF003971>, 2017.
- 605 Mote, T. L.: Greenland surface melt trends 1973–2007: Evidence of a large increase in 2007, *Geophysical Research Letters*, 34, <https://doi.org/10.1029/2007GL031976>, <http://agupubs.onlinelibrary.wiley.com/doi/abs/10.1029/2007GL031976>, _eprint: <https://onlinelibrary.wiley.com/doi/pdf/10.1029/2007GL031976>, 2007.
- Mouginot, J. and Rignot, E.: Ice motion of the Patagonian Icefields of South America: 1984–2014, *Geophysical Research Letters*, 42, 1441–1449, <https://doi.org/10.1002/2014GL062661>, <https://agupubs.onlinelibrary.wiley.com/doi/full/10.1002/2014GL062661>, 2015.
- 610 Nagy, T. and Andreassen, L. M.: Glacier surface velocity mapping with Sentinel-2 imagery in Norway, 2019.

- Nagy, T., Andreassen, L. M., Duller, R. A., and Gonzalez, P. J.: SenDiT: The Sentinel-2 Displacement Toolbox with Application to Glacier Surface Velocities, *Remote Sensing*, 11, 1151, <https://doi.org/10.3390/rs11101151>, <https://www.mdpi.com/2072-4292/11/10/1151>, number: 10 Publisher: Multidisciplinary Digital Publishing Institute, 2019.
- 615 Nye, J. F.: The Mechanics of Glacier Flow, *Journal of Glaciology*, 2, 82–93, <https://doi.org/10.3189/S0022143000033967>, <http://www.cambridge.org/core/journals/journal-of-glaciology/article/mechanics-of-glacier-flow/5FB3C31120796459A837491ACB085F32>, publisher: Cambridge University Press, 1952.
- Nye, J. F.: Glacier sliding without cavitation in a linear viscous approximation, *Proceedings of the Royal Society of London. A. Mathematical and Physical Sciences*, 315, 381–403, publisher: The Royal Society London, 1970.
- 620 Oertel, M. and Süfke, F.: Two-dimensional dam-break wave analysis: particle image velocimetry versus optical flow, *Journal of Hydraulic Research*, 58, 326–334, <https://doi.org/10.1080/00221686.2019.1579114>, <https://doi.org/10.1080/00221686.2019.1579114>, publisher: Taylor & Francis _eprint: <https://doi.org/10.1080/00221686.2019.1579114>, 2020.
- Pfeffer, W. T., Arendt, A. A., Bliss, A., Bolch, T., Cogley, J. G., Gardner, A. S., Hagen, J.-O., Hock, R., Kaser, G., Kienholz, C., Miles, E. S., Moholdt, G., Mölg, N., Paul, F., Radić, V., Rastner, P., Raup, B. H., Rich, J., Sharp, M. J., and Consortium, T. R.: The Randolph Glacier Inventory: a globally complete inventory of glaciers, *Journal of Glaciology*, 60, 537–552, <https://doi.org/10.3189/2014JoG13J176>, <http://www.cambridge.org/core/journals/journal-of-glaciology/article/randolph-glacier-inventory-a-globally-complete-inventory-of-glaciers/730D4CC76E0E3EC1832FA3F4D90691CE>, publisher: Cambridge University Press, 2014.
- 625 Porter, C., Morin, P., Howat, I., Noh, M.-J., Bates, B., Peterman, K., Keesey, S., Schlenk, M., Gardiner, J., Tomko, K., Willis, M., Kelleher, C., Cloutier, M., Husby, E., Foga, S., Nakamura, H., Platson, M., Wethington, M., Williamson, C., Bauer, G., Enos, J., Arnold, G., Kramer, W., Becker, P., Doshi, A., D’Souza, C., Cummins, P., Laurier, F., and Bojesen, M.: ArcticDEM, <https://doi.org/10.7910/DVN/OHHUKH>, <https://dataverse.harvard.edu/dataset.xhtml?persistentId=doi:10.7910/DVN/OHHUKH>, publisher: Harvard Dataverse type: dataset, 2018.
- 630 Rabatel, A., Dedieu, J.-P., Thibert, E., Letréguilly, A., and Vincent, C.: 25 years (1981–2005) of equilibrium-line altitude and mass-balance reconstruction on Glacier Blanc, French Alps, using remote-sensing methods and meteorological data, *Journal of Glaciology*, 54, 307–314, <https://doi.org/10.3189/002214308784886063>, <http://www.cambridge.org/core/journals/journal-of-glaciology/article/25-years-19812005-of-equilibriumline-altitude-and-massbalance-reconstruction-on-glacier-blanc-french-alps-using-remotesensing-methods-and-m>
- 635 DB04ED9DE41C79FCA126917511C8A08E, publisher: Cambridge University Press, 2008.
- Rabatel, A., Sanchez, O., Vincent, C., and Six, D.: Estimation of Glacier Thickness From Surface Mass Balance and Ice Flow Velocities: A Case Study on Argentière Glacier, France, *Frontiers in Earth Science*, 6, <https://doi.org/10.3389/feart.2018.00112>, <https://www.frontiersin.org/articles/10.3389/feart.2018.00112/full>, publisher: Frontiers, 2018.
- 640 Raffel, M., Willert, C. E., Scarano, F., Kähler, C. J., Wereley, S. T., and Kompenhans, J.: Particle Image Velocimetry: A Practical Guide, Springer, google-Books-ID: wk9UDwAAQBAJ, 2018.
- Rhee, J., Im, J., and Carbone, G. J.: Monitoring agricultural drought for arid and humid regions using multi-sensor remote sensing data, *Remote Sensing of Environment*, 114, 2875–2887, <https://doi.org/10.1016/j.rse.2010.07.005>, <http://www.sciencedirect.com/science/article/pii/S003442571000221X>, 2010.
- 645 Rignot, E., Mouginot, J., and Scheuchl, B.: Ice Flow of the Antarctic Ice Sheet, *Science*, 333, 1427–1430, <https://doi.org/10.1126/science.1208336>, <https://science.sciencemag.org/content/333/6048/1427>, publisher: American Association for the Advancement of Science Section: Report, 2011.
- Saberi, L., McLaughlin, R. T., Ng, G.-H. C., Frenierre, J. L., Wickert, A. D., Baraer, M., Zhi, W., Li, L., and Mark, B. G.: Multi-scale temporal variability in meltwater contributions in a tropical glacierized watershed, *Hydrology and Earth System*

- 650 Sciences, 23, 405–425, <https://doi.org/https://doi.org/10.5194/hess-23-405-2019>, <https://www.hydrol-earth-syst-sci.net/23/405/2019/hess-23-405-2019.html>, publisher: Copernicus GmbH, 2019.
- Scambos, M. F. T.: Global Land Ice Velocity Extraction from Landsat 8 (GoLIVE), <https://doi.org/10.7265/N5ZP442B>, <https://nsidc.org/data/nsidc-0710>, type: dataset, 2016.
- Scambos, T. A., Dutkiewicz, M. J., Wilson, J. C., and Bindshadler, R. A.: Application of image cross-correlation to the measurement of
655 glacier velocity using satellite image data, *Remote Sensing of Environment*, 42, 177–186, [https://doi.org/10.1016/0034-4257\(92\)90101-O](https://doi.org/10.1016/0034-4257(92)90101-O), <http://www.sciencedirect.com/science/article/pii/003442579290101O>, 1992.
- Scambos, T. A., Haran, T. M., Fahnestock, M. A., Painter, T. H., and Bohlander, J.: MODIS-based Mosaic of Antarctica (MOA) data sets: Continent-wide surface morphology and snow grain size, *Remote Sensing of Environment*, 111, 242–257, <https://doi.org/10.1016/j.rse.2006.12.020>, <http://www.sciencedirect.com/science/article/pii/S0034425707002854>, 2007.
- 660 Schwalbe, E. and Maas, H.-G.: The determination of high-resolution spatio-temporal glacier motion fields from time-lapse sequences, *Earth Surface Dynamics*, 5, 861–879, <https://doi.org/10.5194/esurf-5-861-2017>, <https://www.earth-surf-dynam.net/5/861/2017/>, 2017.
- Sevestre, H. and Benn, D. I.: Climatic and geometric controls on the global distribution of surge-type glaciers: implications for a unifying model of surging, *Journal of Glaciology*, 61, 646–662, <https://doi.org/10.3189/2015JoG14J136>, <http://www.cambridge.org/core/journals/journal-of-glaciology/article/>
665 climatic-and-geometric-controls-on-the-global-distribution-of-surgetype-glaciers-implications-for-a-unifying-model-of-surging/
34D15501CBBF803608401FEAA6B0FC61, publisher: Cambridge University Press, 2015.
- Shean, D.: dshean/vmap: Zenodo DOI release, <https://doi.org/10.5281/zenodo.3243479>, <https://zenodo.org/record/3243479#.XwiOvihKhPY>, 2019.
- Sneed, W. A. and Hamilton, G. S.: Evolution of melt pond volume on the surface of the Greenland Ice Sheet, *Geophysical*
670 *Research Letters*, 34, <https://doi.org/10.1029/2006GL028697>, <http://agupubs.onlinelibrary.wiley.com/doi/abs/10.1029/2006GL028697>,
_eprint: <https://onlinelibrary.wiley.com/doi/pdf/10.1029/2006GL028697>, 2007.
- Stearns, L. A., Smith, B. E., and Hamilton, G. S.: Increased flow speed on a large East Antarctic outlet glacier caused by subglacial floods, *Nature Geoscience*, 1, 827–831, <https://doi.org/10.1038/ngeo356>, <http://www.nature.com/articles/ngeo356>, number: 12 Publisher: Nature Publishing Group, 2008.
- 675 Stocker, T. F., Qin, D., Plattner, G.-K., Tignor, M., Allen, S. K., Boschung, J., Nauels, A., Xia, Y., Bex, V., and Midgley, P. M.: Climate change 2013: The physical science basis, Contribution of working group I to the fifth assessment report of the intergovernmental panel on climate change, 1535, publisher: Cambridge university press Cambridge, United Kingdom and New York, NY, USA, 2013.
- Sveen, J. K.: An introduction to MatPIV v. 1.6.1, <https://www.duo.uio.no/handle/10852/10196>, accepted: 2013-03-12T08:18:23Z Publisher: Matematisk Institutt, Universitetet i Oslo, 2004.
- 680 Sveen, J. K. and Cowen, E. A.: Quantitative imaging techniques and their application to wavy flows, in: PIV and Water Waves, vol. Volume 9 of *Advances in Coastal and Ocean Engineering*, pp. 1–49, WORLD SCIENTIFIC, https://doi.org/10.1142/9789812796615_0001, https://www.worldscientific.com/doi/abs/10.1142/9789812796615_0001, 2004.
- Thielicke, W. and Stamhuis, E.: PIVlab – Towards User-friendly, Affordable and Accurate Digital Particle Image Velocimetry in MATLAB, *Journal of Open Research Software*, 2, e30, <https://doi.org/10.5334/jors.bl>, <http://openresearchsoftware.metajnl.com/articles/10.5334/jors.bl/>, number: 1 Publisher: Ubiquity Press, 2014.
- 685

- Thompson, L. G., Mosley-Thompson, E., Davis, M. E., and Brecher, H. H.: Tropical glaciers, recorders and indicators of climate change, are disappearing globally, *Annals of Glaciology*, 52, 23–34, <https://doi.org/10.3189/172756411799096231>, https://www.cambridge.org/core/product/identifier/S0260305500250957/type/journal_article, 2011.
- Tralli, D. M., Blom, R. G., Zlotnicki, V., Donnellan, A., and Evans, D. L.: Satellite remote sensing of earthquake, volcano, flood, landslide and coastal inundation hazards, *ISPRS Journal of Photogrammetry and Remote Sensing*, 59, 185–198, <https://doi.org/10.1016/j.isprsjprs.2005.02.002>, <http://www.sciencedirect.com/science/article/pii/S0924271605000043>, 2005.
- Van Wyk de Vries, M.: Glacier Image Velocimetry (GIV), <https://doi.org/10.5281/zenodo.4159875>, <https://zenodo.org/record/4144839#.X517OtD7RPY>, 2020a.
- Van Wyk de Vries, M.: Glacier Image Velocimetry (GIV) app, <https://doi.org/10.5281/zenodo.4147589>, <https://zenodo.org/record/4144854#.X517Z9D7RPY>, 2020b.
- Vergara, W., Deeb, A., Valencia, A., Bradley, R., Francou, B., Zarzar, A., Grünwaldt, A., and Haeussling, S.: Economic impacts of rapid glacier retreat in the Andes, *Eos, Transactions American Geophysical Union*, 88, 261–264, <https://doi.org/10.1029/2007EO250001>, <http://agupubs.onlinelibrary.wiley.com/doi/abs/10.1029/2007EO250001>, [_eprint: https://onlinelibrary.wiley.com/doi/pdf/10.1029/2007EO250001](https://onlinelibrary.wiley.com/doi/pdf/10.1029/2007EO250001), 2007.
- Wal, R. S. W. v. d., Boot, W., Broeke, M. R. v. d., Smeets, C. J. P. P., Reijmer, C. H., Donker, J. J. A., and Oerlemans, J.: Large and Rapid Melt-Induced Velocity Changes in the Ablation Zone of the Greenland Ice Sheet, *Science*, 321, 111–113, <https://doi.org/10.1126/science.1158540>, <https://science.sciencemag.org/content/321/5885/111>, publisher: American Association for the Advancement of Science Section: Report, 2008.
- Weertman, J.: On the Sliding of Glaciers, *Journal of Glaciology*, 3, 33–38, <https://doi.org/10.3189/S0022143000024709>, <http://www.cambridge.org/core/journals/journal-of-glaciology/article/on-the-sliding-of-glaciers/E16342853EE9ED61ED1CDE79FE3BF4C5>, publisher: Cambridge University Press, 1957.
- Wickert, A. D.: The ALog: Inexpensive, Open-Source, Automated Data Collection in the Field, *The Bulletin of the Ecological Society of America*, 95, 166–176, <https://doi.org/10.1890/0012-9623-95.2.68>, <https://esajournals.onlinelibrary.wiley.com/doi/abs/10.1890/0012-9623-95.2.68>, [_eprint: https://esajournals.onlinelibrary.wiley.com/doi/pdf/10.1890/0012-9623-95.2.68](https://esajournals.onlinelibrary.wiley.com/doi/pdf/10.1890/0012-9623-95.2.68), 2014.
- Wickert, A. D., Sandell, C. T., Schulz, B., and Ng, G.-H. C.: Open-source Arduino-compatible data loggers designed for field research, *Hydrology and Earth System Sciences*, 23, 2065–2076, <https://doi.org/https://doi.org/10.5194/hess-23-2065-2019>, <https://www.hydrol-earth-syst-sci.net/23/2065/2019/>, publisher: Copernicus GmbH, 2019.
- Willis, M. J., Zheng, W., Durkin, W. J., Pritchard, M. E., Ramage, J. M., Dowdeswell, J. A., Benham, T. J., Bassford, R. P., Stearns, L. A., Glazovsky, A. F., Macheret, Y. Y., and Porter, C. C.: Massive destabilization of an Arctic ice cap, *Earth and Planetary Science Letters*, 502, 146–155, <https://doi.org/10.1016/j.epsl.2018.08.049>, <http://www.sciencedirect.com/science/article/pii/S0012821X18305156>, 2018.
- Wright, R., Flynn, L., Garbeil, H., Harris, A., and Pilger, E.: Automated volcanic eruption detection using MODIS, *Remote Sensing of Environment*, 82, 135–155, [https://doi.org/10.1016/S0034-4257\(02\)00030-5](https://doi.org/10.1016/S0034-4257(02)00030-5), <http://www.sciencedirect.com/science/article/pii/S0034425702000305>, 2002.
- Yuwei, W. U., Jianqiao, H. E., Zhongming, G. U. O., and Anan, C.: Limitations in identifying the equilibrium-line altitude from the optical remote-sensing derived snowline in the Tien Shan, China, *Journal of Glaciology*, 60, 1093–1100, <https://doi.org/10.3189/2014JoG13J221>, <http://www.cambridge.org/core/journals/journal-of-glaciology/article/limitations-in-identifying-the-equilibriumline-altitude-from-the-optical-remotesensing-derived-snowline-in-the-tien-shan-china/6B84B734744312D483016C99C6373356>, publisher: Cambridge University Press, 2014.

- 725 Zheng, W., Pritchard, M. E., Willis, M. J., Tepes, P., Gourmelen, N., Benham, T. J., and Dowdeswell, J. A.: Accelerating glacier mass loss on Franz Josef Land, Russian Arctic, *Remote Sensing of Environment*, 211, 357–375, <https://doi.org/10.1016/j.rse.2018.04.004>, <http://www.sciencedirect.com/science/article/pii/S0034425718301494>, 2018.
- Zheng, W., Durkin, W. J., Melkonian, A. K., and Pritchard, M. E.: Cryosphere And Remote Sensing Toolkit (CARST) v1.0.1, <https://doi.org/10.5281/zenodo.3475693>, <https://zenodo.org/record/3475693#.XvSuS2hKhPZ>, 2019a.
- 730 Zheng, W., Pritchard, M. E., Willis, M. J., and Stearns, L. A.: The Possible Transition From Glacial Surge to Ice Stream on Vavilov Ice Cap, *Geophysical Research Letters*, 46, 13 892–13 902, <https://doi.org/10.1029/2019GL084948>, <http://agupubs.onlinelibrary.wiley.com/doi/abs/10.1029/2019GL084948>, _eprint: <https://onlinelibrary.wiley.com/doi/pdf/10.1029/2019GL084948>, 2019b.

Table 1. Non-exhaustive list of codes and toolboxes that may be used for feature tracking, and associated references. 3-1 = fully available, 2 = available, but relies on commercial software, +3 = not available. A spreadsheet with download links is available in the supplementary material.

Toolbox	Source	Summary	Availiability
Auto-RIFT	Gardner et al. (2018)	Python dense feature-tracking <u>feature-tracking</u> package for calculating displacement from optical or radar imagery. Used for calculating the ITS_LIVE global velocity dataset.	<u>3-1</u>
CARST	Zheng et al. (2019a)	Python and bash scripts for feature tracking and ice elevation change analysis.	<u>3-1</u>
CIAS	Kääb and Vollmer (2000)	IDL based correlation software to compute offsets between two images.	<u>3-1</u>
Cosi-Corr	Leprince et al. (2007a)	IDL/ENVI based package for image co-registration and displacement mapping.	2
EMT	Schwalbe and Maas (2017)	Workflow for analysis and feature tracking of time-lapse ground based imagery.	<u>3-1</u>
GIV	This study.	GUI based feature-tracking <u>feature-tracking</u> toolbox for glaciology.	<u>3-1</u>
fourDvel	Minchew et al. (2017)	Fortran routine for calculation of 3d velocity fields from geolocated displacement data.	<u>3-1</u>
ImCorr	Scambos et al. (1992)	C and Fortran package for dense feature tracking of satellite or airphoto imagery.	<u>3-1</u>
ImGRAFT	Messerli and Grinsted (2015)	MATLAB based package for georectification of ground-based imagery and feature tracking.	2
matpiv <u>MatPIV</u>	Sveen (2004)	MATLAB based toolbox for pattern matching and particle image velocimetry (PIV).	2
PIVlab	Thielicke and Stamhuis (2014)	GUI based MATLAB PIV toolbox	2
Pointcatcher	James et al. (2016)	MATLAB based toolbox for facilitating manual feature tracking in image time-series.	2
PyCorr	Fahnestock et al. (2016)	Python based feature-tracking <u>feature-tracking</u> toolbox. Used for calculating the GoLIVE global velocity dataset.	<u>+3</u>
PyTrx	How et al. (2020)	Python toolbox created for calculating displacements from oblique images and time-lapse image series.	<u>3-1</u>
SendIT	Nagy et al. (2019)	Flexible processing toolbox for retrieval of glacier surface velocities, based on ImCorr.	<u>3-1</u>
vmap	Shean (2019)	Ames Stereo Pipeline based image correlator for velocity map generation.	<u>3-1</u>